A NOVEL APPROACH FOR FABRICATION OF FREE-STANDING CONDUCTIVE NETWORK: PEDOT:PSS BASED BENDABLE CHEMO AND PHOTORESISTOR

A Thesis Submitted to
the Graduate School of Engineering and Sciences of
İzmir Institute of Technology
in Partial Fulfillment of the Requirements for the Degree of

MASTER OF SCIENCE

in Materials Science and Engineering

by
Mustafa Umut MUTLU

June 2019
İZMİR

We approve the thesis of **Mustafa Umut MUTLU**

Examining Committee Members:

Assoc. Prof. Dr. Ümit Hakan YILDIZ
Department of Chemistry, İzmir Institute of Technology

Assoc. Prof. Dr. Cem ÇELEBİ
Department of Physics, İzmir Institute of Technology

Assist. Prof. Dr. Gökhan UTLU
Department of Physics, Ege University

26 June 2019

Assoc. Prof. Dr. Ümit Hakan YILDIZ
Supervisor, Department of Chemistry
İzmir Institute of Technology

Prof. Dr. Mustafa M. DEMİR
Co-Supervisor, Department of
Materials Science and Engineering
İzmir Institute of Technology

Assoc. Prof. Dr. Hâldun SEVİNÇLİ
Head of the Department of Materials
Science and Engineering

Prof. Dr. Aysun SOFUOĞLU
Dean of the Graduate School of
Engineering and Science

ACKNOWLEDGMENTS

I would like to acknowledge the help of many people who have been there during the course of my study. Firstly, I would like to express my sincere gratitude to my advisor Assoc. Prof. Dr. Ümit Hakan YILDIZ and co-supervisor Prof. Dr. Mustafa M. DEMİR for their guidance, suggestions, patience, encouragement and support throughout my thesis study.

I am also thankful to Assoc. Prof. Dr. Cem ÇELEBİ and Assist. Prof. Gökhan UTLU who willingly accepted to be members of my thesis examining committee, Assist. Prof. Dr. Osman AKIN and Prof. Dr. Canan VARLIKLI for their constructively suggestions and comments on this project.

In addition, I also thank to the specialists at IZTECH - Center of Materials Research for the SEM analysis and The Scientific and Technological Research Council of Turkey (TÜBİTAK) for the support of this work through the project 117F243.

I am really thankful to Hande UÇAK, İrem ACAR and Melis EMRE for their cooperation and support during part of the thesis.

I would like to thank to lovely and engaging mates Cemre YAŞAR, Dilce ÖZKENDİR, Duygu ERDOĞAN, Esra TÜRKER, Müge YÜCEL, Öykü YILDIRIMKARAMAN, Sezer ÖZENLER and all the members of BioSens & BioApps and Biomimetics groups for their help when I need. They have listened to me without being tired and always support me and encouragement me in any case. We had good times together and I wish them successful and happy tomorrows.

Finally, I would like to offer my special thanks to my parents and my dearest for their love, being in my behind, always trusting, supporting and encouraging me in every moment of my life. I am very lucky to have them. I love them so much and dedicate my thesis to my family.

ABSTRACT

A NOVEL APPROACH FOR FABRICATION OF FREE-STANDING CONDUCTIVE NETWORK: PEDOT:PSS BASED BENDABLE CHEMO AND PHOTORESISTOR

Electrospinning is a simple and versatile technique for the fabrication of polymeric nanofibrous substrate with high surface to volume ratio. Besides high surface to volume ratio, their dimensional stability and flexibility make it a perfect candidate for conductive network for various sensor applications. Free-Standing conductive network can be fabricated by deposition of PEDOT:PSS or MWCNT through bendable nanofibrous substrate. As a simple example for sensor applications, the moving object has been sensed through the electrostatic interactions between fibers and object. The sensing range has been found to be 1-5 cm above the surface of fabric. By the controlled combination of conductive polymers and electrospun polymer nanofibers effective device miniaturization has been provided without loss of performance. The noncontact motion sensor platform has unique flexibility and light weight holding a potential for wearable sensor technology. For another application as a wearable electronics, the controlled combination of conductive network and light-matter interaction provides opportunities to fabricate photo-resistor exhibits broad band response 400 to 1600 nm that holding promises for ultra-thin sensors used in telecommunication. As a final example, we report the effect of gold and iron oxide nanoparticles on the selectivity and sensitivity of MWCNT or PEDOT:PSS based chemiresistor responsive to VOCs. The interplay between conductive layer by gold and iron oxide nanoparticles resulted a significant conductivity improvement that affecting selectivity which is governed by the interaction between electron-donating VOCs and NP doped conductive layer due to variation in charge carrier densities in conductive layer lattice.

ÖZET

BAĞIMSIZ İLETKEN AĞ ÜRETİMİ İÇİN YENİ BİR YAKLAŞIM: PEDOT:PSS TABANLI BÜKÜLEBİLİR KEMO VE FOTO DİRENÇ

Elektroeğirme, çap ölçüleri nanometreden mikrometreye kadar değişebilen polimerik lif üretiminde kullanılan basit ve çok yönlü bir yöntemdir. Son derece küçük çap ölçüleri nedeniyle, yüksek yüzey/hacim oranına sahip olan elektroeğirme nanolifler, aynı zamanda yapısal olarak sağlam ve esnek yapılardır. Bu özelliklerine bağlı olarak, elektroeğirme yöntemi ile üretilen nanolifler, birçok bükülebilir sensör uygulamaları için önemli bir adaydır. Elektroeğirme ile üretilen bükülebilir nanoliflerin üzerine PEDOT:PSS veya MWCNT ile modifiye ederek bağımsız iletken ağı üretmek mümkündür. Sensör uygulamalarına örnek olarak, yapılan çalışmalar ile sensör yüzeyinin üstünde hareket eden objenin algılanabildiği gözlemlenmiştir. Objenin algılanması, sensör ile nesne arasındaki elektrostatik etkileşimler sayesinde olmaktadır. Bu sayede 1 – 5 cm mesafedeki nesneler algılanabilir. İletken polimer ve nanoliflerin birleşimi ile dengeli iletken ağ oluşturarak performans kaybı olmadan ufak boyutlu sensör üretilebilir. Üretilen sensör, hafifliği ve esnekliği ile giyilebilir elektronik uygulamalarında kullanılabilir. Uygulanan bir başka giyilebilir elektronik örneğinde, telekomünikasyon sektöründe kullanılabilecek iletken ağın ışık ile etkileşimi sayesinde 400 – 1600 nm aralığındaki dalga boylarını algılayabilen foto direnç üretilebilir. Son olarak, demir ve altın nano parçacıkların uçucu organik bileşiklerin tayininde seçiciliğe ve hassasiyetine etkileri araştırıldı. İletken ağ ile nano parçacıkların etkileşimi sensörün iletkenliğini arttırarak organik uçucu gaz seçiciliğini etkilemekte. Organik uçucu gaz seçiciliği ise elektron veren organik uçucu gazlar ile nano parçacık ile katkılanmış iletken ağın etkileşimlerinden kaynaklanmaktadır.

TABLE OF CONTENTS

LIST OF FIGURES

Figure **Page**

Figure **Page**

Figure **Page**

LIST OF ABBREVATIONS

AFM	Atomic Force Microscopy
AuNP	Gold Nanoparticle
DC	Direct Current
DMF	Dimethylformamide
FeNP	Iron Oxide Nanoparticle
FET	Field Effect Transistor
FSO	Full Scale Output
H_2O_2	Hydrogen Peroxide
H_2SO_4	Sulfuric Acid
HCl	Hydrochloric Acid
HNO_3	Nitric Acid
MWCNT	Multi Walled Carbon Nanotube
NH_4OH	Ammonium Hydroxide
NIR	Near Infrared
NP	Nanoparticle
PA	polyacetylene
PANI	Polyaniline
PCB	Printed Circuit Board
PEDOT:PSS	Poly(3,4-ethylenedioxythiophene):poly(styrenesulfonate)
PET	(Poly(ethylene terephthalate)
P-I-D	proportional–integral–derivative
PMMA	Poly(methyl methacrylate)
PP	Poly(p-phenylene)
PPy	Polypyrrole
PPV	Poly(p-phenylene vinylene)
PT	Polythiophene
RPM	Revolution Per Minute
SEM	Scanning Electron Microscopy
UV	Ultraviolet
VOC	Volatile Organic Compound
ZnO	Zinc Oxide

CHAPTER 1

INTRODUCTION

1.1. Scope of the Thesis

Fabricating polymer based conductive network has been taking attention in sensor technologies (Adhikari & Majumdar, 2004; Huang, Zhang, Kotaki, & Ramakrishna, 2003; Janata & Josowicz, 2003). Particularly, PEDOT:PSS and CNT based conductive bulk materials are excellent candidates for sensor application such as; motion sensing, photosensors or VOC sensors (Drummond, Hill, & Barton, 2003; Li et al., 2003; Someya et al., 2004). Furthermore, sensing characteristics can be altered via doping with NPs (Mutlu, Akin, & Yildiz, 2018; Tasaltin & Basarir, 2014).

1.2. Sensor technology

In terms of instrumentation, an electrical sensor is a device that convert non-electrical signals (temperature, humidity, blood pressure, etc.) to electrical outputs. Such that, they may think as a binder between the physical world and the world of electrical devices. Inversely, actuators are the ones that convert electrical signals into physical phenomena (Wilson, 2005).

These days, a variety of sensors has been developed are polymers. Thanks to the characteristics of their chemical and physical properties they can adapt to many applications. In the last two decades, tremendous interest has been shown in polymeric materials that could reversibly or irreversibly change their physical and chemical properties under the influence of external stimuli such as; pH, temperature, light radiation, magnetic field, light radiation, mechanical forces, magnetic fields, electric fields, and bioactive molecules (Gong et al., 2009; Lange, Roznyatouskaya, & Mirsky, 2008). Smart polymers may come in the form of solutions, gels, self-assembled nanoparticles, films, or solids (Lin & Yan, 2012; Richter et al., 2008). Researchers have been trying to use already known features of such materials in more complex issues, such as adaptive coatings, controlled delivery of drugs and genes, catalysis, detection and imaging or adaptive

coatings (Alexeev et al., 2003; Delcea, Mohwald, & Skirtach, 2011). Intelligent materials based on polymers exhibit a number of advantages in terms of structural stability, dispersion in aqueous solutions, biocompatibility, ease of processing and subsequent integration with detection devices (Cichosz, Masek, & Zaborski, 2018; Hu & Liu, 2010).

1.2.1. Sensor Performance Characteristics Definitions

The following are some of the important sensor characteristics according to Carr et. al. (Carr, 1993):

1.2.1.1. Transfer Function

Transfer function is the relationship between physical input and electrical output signal that generally represented as a graph showing the functional relationship between input and output signal where there may be formulation about the conversion. The formulation is used to predict the behavior of the sensor and contains information about the sensitivity and the offset at the output of the sensor.

1.2.1.2. Sensitivity

Sensitivity is defined as the relationship between physical signal input and electrical signal output. It is generally the ratio between a small change in electrical signal to a small change in physical signal. Likewise, it may be expressed as the derivative of the transfer function with respect to physical signal. For example, a thermometer would have “high sensitivity” if a small temperature change resulted in a large voltage change. The sensitivity may in practice differ from the value specified. This is called a sensitivity error. Sensitivity error is the relative deviation (%) of the slope of the line through these points, compared to the optimum, or the zero-deviation slope.

1.2.1.3. Dynamic Range (Span)

The range of input physical signals that may be converted to electrical signals by the sensor is the dynamic range or span. While in the range, the signal has to be converted to the electrical output where the transfer formulation stands. If the input signal is outside the range, electrical output is expected to irrefutably inaccurate. Dynamic range is usually defined by the supplier as the range over which other performance characteristics described in the data sheets are expected to apply.

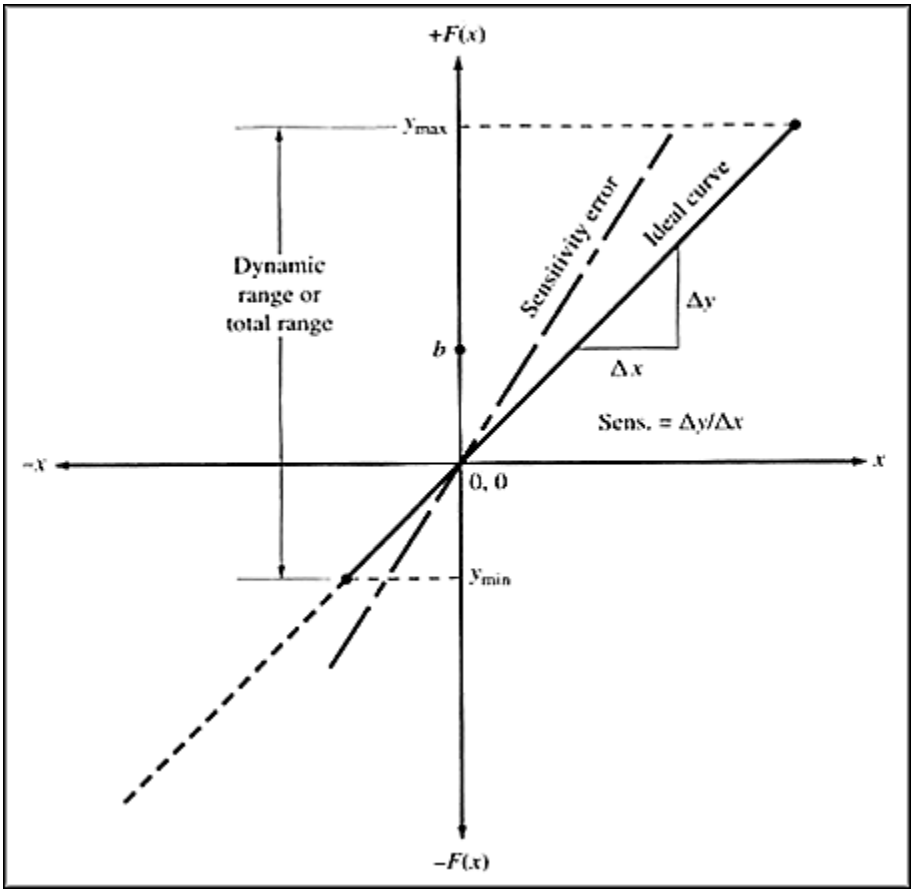

Figure 1. Ideal curve and sensitivity error (Source: Carr, 1993)

1.2.1.4. Accuracy or Uncertainty

The accuracy of the sensor is the maximum deviation of the indicated value that will exist from the actual value at the output of the sensor. The accuracy can be expressed either as a percentage of full scale or in absolute terms. For example, a thermometer might be guaranteed accurate to within 5% of FSO. Accuracy is generally considered by meteorologists to be a qualitative term, while uncertainty is quantitative. For example, one sensor might have better accuracy than another if its uncertainty is 1% compared to the other with an uncertainty of 3%.

1.2.1.5. Hysteresis

Some sensors do not return to the same output value when the input stimulus is cycled up or down. The width of the expected error in terms of the measured quantity is defined as the hysteresis.

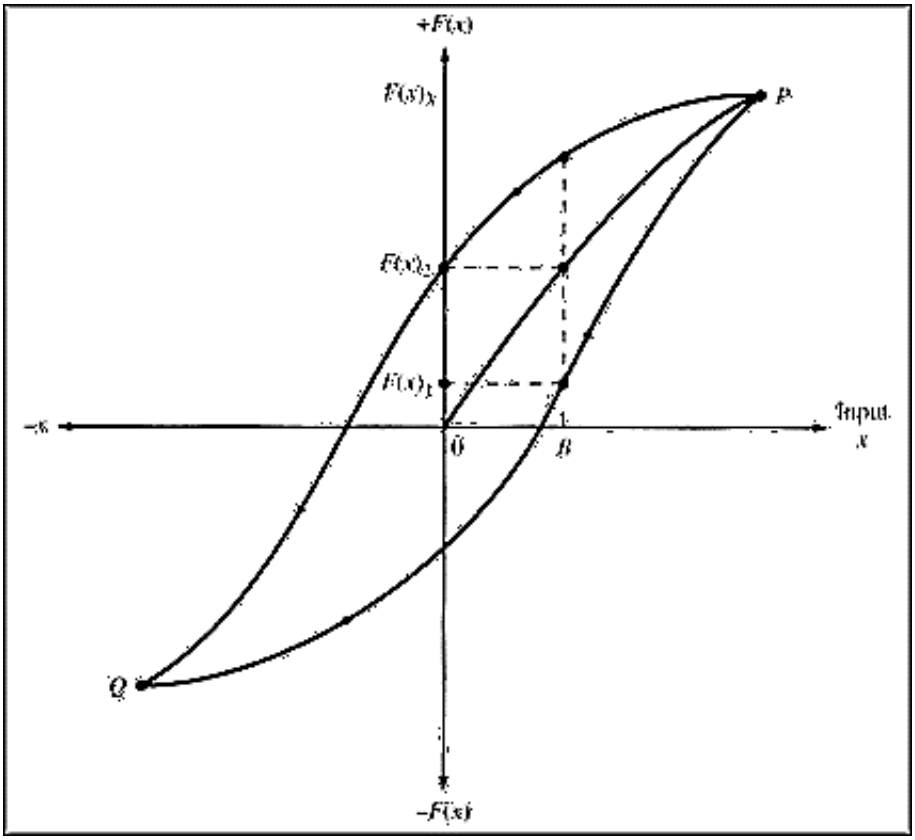

Figure 2. Hysteresis curve (Source: Carr, 1993)

1.2.1.1. Nonlinearity (Linearity)

Linearity error is the deviation of the sensor output curve from a specified straight line over the specified dynamic range. This linearity error is also defined as non-linearity which is the maximum deviation from a linear transfer function over the range. Figure 3 shows the relationship between the ideal line and the actual measured or calibration line. Linearity is often specified in terms of percentage of nonlinearity, which is defined as:

$$Nonlinearity\ (\%)\ =\ \frac{D_{in(max)}}{\mathrm{IN}_{f.s}}\times 100$$

where

Nonlinearity (%) : The percentage of nonlinearity

$D_{in(max)}$: The maximum input deviation

$IN_{f.s.}$: The maximum, full-scale input

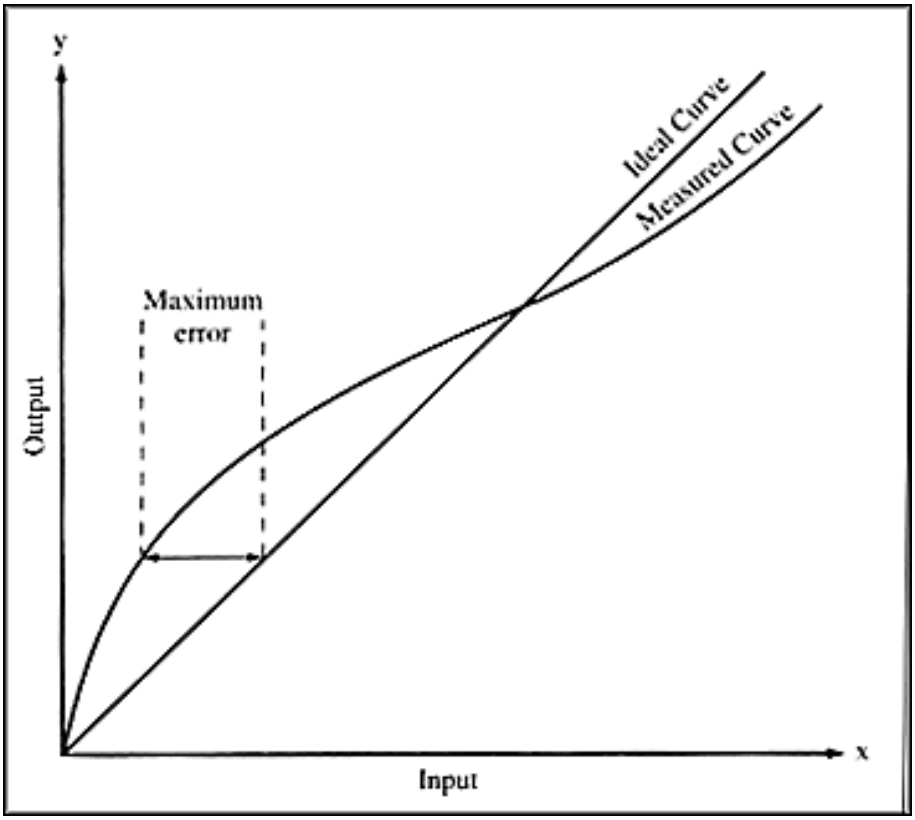

Figure 3. Ideal versus measured curve showing linearity error (Source: Carr, 1993)

1.2.1.2. Noise

All sensors produce some output noise in addition to the output signal. In many cases the noise of the sensor limits the performance of the system based on the sensor. Noise is generally distributed across the frequency spectrum. The standard deviation value of the noise strength is an important factor in measurements. The mean value of the signal divided by this value gives a good benchmark, as how readily the information can be extracted. As a result, signal-to-noise ratio (S/N) is a commonly used in sensing applications which is defined as:

$$\frac{S}{N} = \frac{\text{Mean value of signal}}{\text{Standard deviation of noise}}$$

Many common noise sources produce a white noise distribution which is the spectral noise density is the same at all frequencies. Johnson noise in a resistor is a good example of such a noise distribution which is the electronic noise generated by the thermal agitation of the charge carriers (generally the electrons) inside a conductor at equilibrium,

which happens regardless of any applied bias. A distribution of this nature adds noise to a measurement with amplitude proportional to the square root of the measurement bandwidth. In other words, there is an inverse relationship between the bandwidth and measurement time. Such that, the noise decreases with the square root of the measurement time.

1.2.1.3. Resolution

Resolution is the minimum detectable signal fluctuation apart from noise. In other words, it is the smallest detectable incremental change of input parameter that can be detected in the output signal. Resolution can be expressed either as a proportion of the reading or in absolute terms.

1.2.1.4. Bandwidth

All sensors have finite response times to an instantaneous change in physical signal. In addition, many sensors have decay times, which would represent the time after a step change in physical signal for the sensor output to decay to its original value. The reciprocal of these times corresponds to the upper and lower cutoff frequencies, respectively. The bandwidth of a sensor is the frequency range between these two frequencies.

1.3. Conjugated Polymers

Polymers are traditionally used as an electric insulators that literally replaced their role as conductors with a range of novel applications (Gong et al., 2009; Yucel et al., 2018). Many researchers in variety of disciplines have an attention to study organic solids that exhibit outstanding conducting properties. A new class of polymers known as conjugated polymers or intrinsically conducting polymers has recently emerged, which exhibit interesting electrical and optical properties hitherto found only in inorganic systems. A crucial requirement for a polymer to become conductive is that there should be an overlap of molecular orbitals to allow the formation of delocalized molecular wave function. Besides this, molecular orbitals must be partially filled so that there is a free movement of electrons throughout the lattice (Bloor & Movaghar, 1983). Figure 4 depicts the extensively studied conjugated polymers.

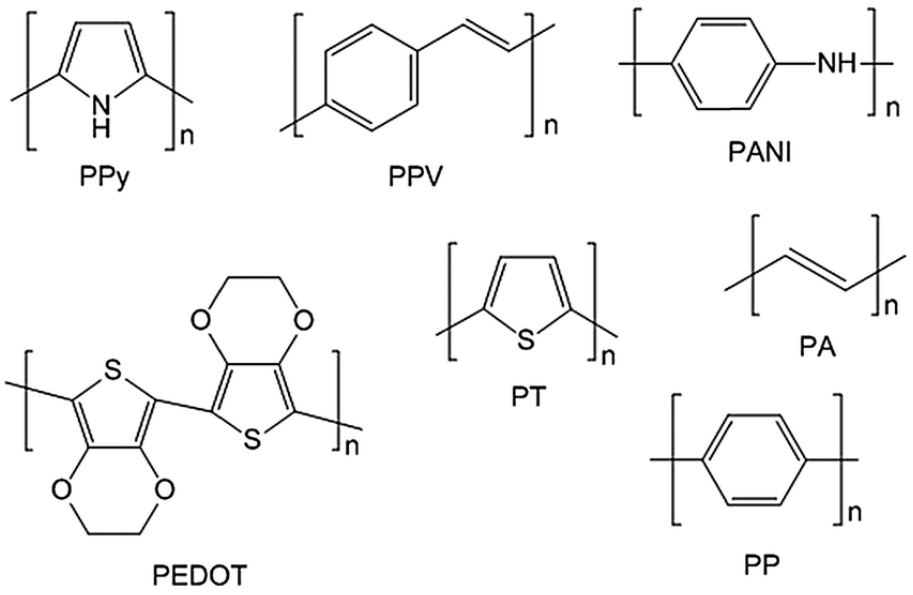

Figure 4. Molecular structures of extensively studied conjugated polymers

Conducting polymers contain π-electron backbone responsible for their fascinating properties such as electrical conductivity, low ionization potential, low energy optical transitions and high electron affinity. This π-conjugated system of the conducting polymers consists of single and double bonds alternating along the polymer chain. The higher values of the electrical conductivity obtained in such organic polymers have led to the name 'synthetic metals'.

Among conjugated polymers, PEDOT steps forward based on its high conductivity, stability and optical transparency in the conducting state. Even though PEDOT is unlikely to cast into films due to its insoluble nature in aqueous media, synthetization with PSS lead to constitute well dispersed aqueous solution. PEDOT:PSS complex **(**Figure 5**)** consist of polycationic, polythiophene derivative, PEDOT and insulator polyanionic PSS salt. PEDOT chains are incorporated into a polyanionic PSS matrix to compensate the charges. By doping PSS, PEDOT becomes hole conductive and it is used as a hole injection layer in organic electronics.

The discovery of CNTs in 1991 (Iijima, 1991) has an important interest to explore the unique electrical and structural characteristics among the researches. CNTs are basically armchair or zigzag formed graphene planes that rolled up and formed single or multi-layered CNTs as shown in Figure 6 (Kan, Yang, & Li, 2011). In particular, high surface to volume ratio and excellent electrical properties that can be easily perturbed with interacting with VOCs (Albanese, Tang, & Chan, 2012). Therefore, MWCNTs are

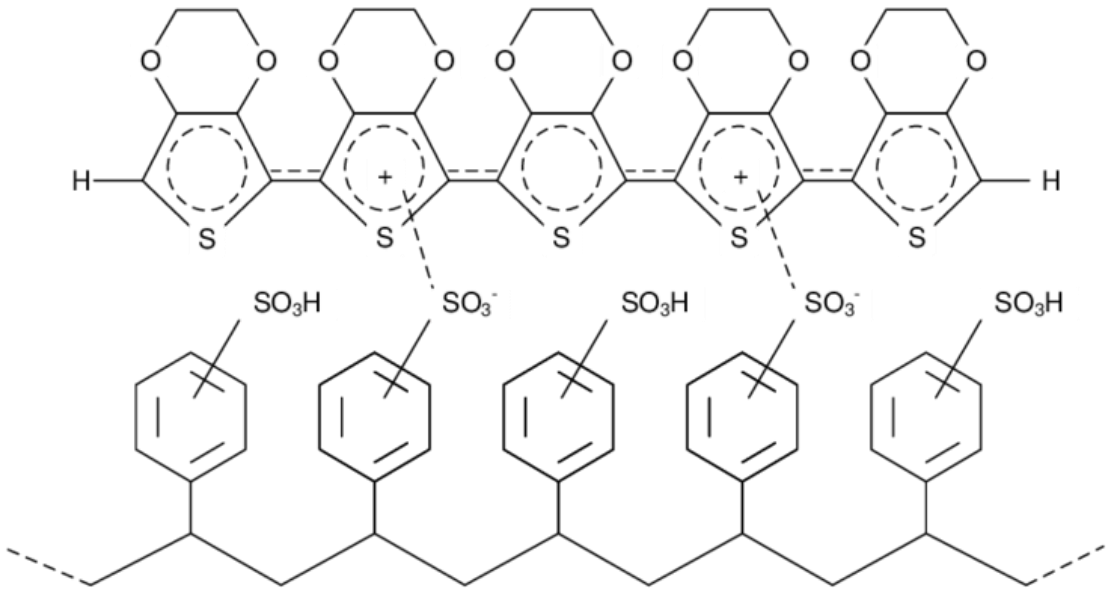

Figure 5. Chemical structure of PEDOT (top) and PSS (bottom)

a promising material to detect active elements for gas-sensing devices. However, gas sensor based on pristine MWCNT have certain limitations. The response of unmodified MWCNTs to analytes is weak, scarcely selective and irreversible. To overcome these limitations, the functionalization of MWCNT is mandatory important both enhance sensitivity and selectivity to analytes (S. Peng & Cho, 2003). Additionally, functionalization of MWCNTs with metal nanoparticles (NPs), due to its extraordinary catalytic properties, enhance the sensor selectivity and sensitivity considerably (Rao et al., 2017). Interaction between VOCs and MWCNT results in electronic charge transfer between gas molecule and sensor which change the conductivity of detection unit. This fact is the one that, depending on the type of metal NP, it is possible to enhance sensitivity and selectivity based on the change in material resistance upon different VOCs.

1.4. Conjugated Polymers in Sensor Applications

Some of the sensor applications were listed below:

1.4.1. Motion Sensors

Pressure sensors with high sensitivity, low operating power, and flexible properties play a critical role in the development of the next-generation flexible electronic devices such as rollable displays, electronic skin (e-skin) sensors and health-care monitoring devices.

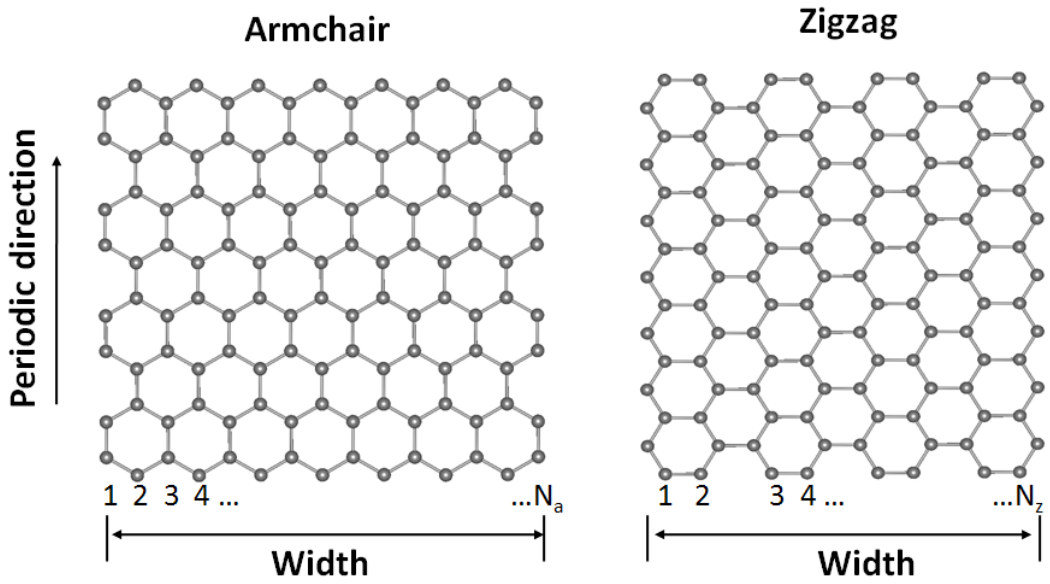

Figure 6. Structure of armchair and zigzag nanoribbons that rolled up to form CNT (Source: Kan, Yang, & Li, 2011)

The specific requirements on sensitivity, response time and operating frequency of these sensors will vary depending upon application. Pressure sensors with high sensitivity can also be used to measure very slight movement of objects or the human body, which would induce pressure changes on the devices. Even if the stress variation or the body movement is very small, pressure sensors can capture the signal and convert it into electrical or mechanical outputs, and thus these body motion sensors would serve as effective communication tools for the patients who suffer from paralysis due to stroke or spinal cord damage.

1.4.2. Photodetectors

Photo detectors are used primarily as an optical receiver to convert light into electricity. The principle that applies to photo detectors is the photoelectric effect, which is the effect on a circuit due to light. Max Planck in 1900 discovered that energy is radiated in small discrete units called quanta; he also discovered a universal constant of nature which is known as the Planck's constant. Planck's discoveries lead to a new form of physics known as quantum mechanics and the photoelectric effect E = hv which is Planck constant multiplied by the frequency of radiation. The photo electric effect is the effect of light on a surface of metal in a vacuum, the result is electrons being ejected from the surface this explains the principle theory of light energy that allows photo detectors to

operate. Photo detectors are commonly used as safety devices in homes in the form of a smoke detector, also in conjunction with other optical devices to form security systems.

1.4.3. Gas Sensors

During the past decade, there was a tremendous effort for VOC detection in human breath for various disease such as lung cancer (G. Peng, Tisch, Adams, et al., 2009), ovarian cancer (Amal et al., 2015), melanoma (D'Amico et al., 2008) or asthma (Montuschi et al., 2010). In particular, Daneshkhah et al. proposed a novel composite sensor comprised of PVDF-HFP/C65/CNT that spin coated on gold over SiO surface (Daneshkhah, Shrestha, Agarwal, & Varahramyan, 2015). They tested their sensor with acetone, water, ethanol, isoprene, and 2-EHA (Ethylhexyl acrylate) by exposing volatilomes and nitrogen in order. Highest resistance change of sensor was achieved 17.9 % by exposing acetone. In addition to this study, Zilberman and co-workers fabricated a random network sponge-like CNT chemiresistor for noninvasive lung cancer diagnosis by investigating the variation of nonpolar VOCs in human breath (Zilberman et al., 2009). They successfully distinguished volatilomes from each other. Peng et al. studied FET based CNT random network sensor array to detect lung cancer and kidney diseases (G. Peng, Tisch, & Haick, 2009). They reported that patients who has chronic renal failure disease was distinguished from healthy breath samples at different relative humidity level at ppm concentration. These examples highlight the capability of CNT based VOC sensor in disease diagnosis. Herein, we report a novel approach to alter selectivity and sensitivity of CNT based chemiresistive sensor by doping metal nanoparticles.

1.5. Electrospinning

Electrospinning technique was firstly discovered by J. Doshi and D. Reneker in 1995 (Doshi & Reneker, 1995). They explained the technique as “An electric field is used to create a charged jet of polymer solution. As this jet travels in air, the solvent evaporates leaving behind a charged fiber that can be electrically deflected or collected on a metal screen”. Electrospinning produce fibrous polymers with a variety of size and shape. Nano or micro-sized and homogenous fibers, also porous, film or sphere structure of polymers can be controllably obtained by this technique.

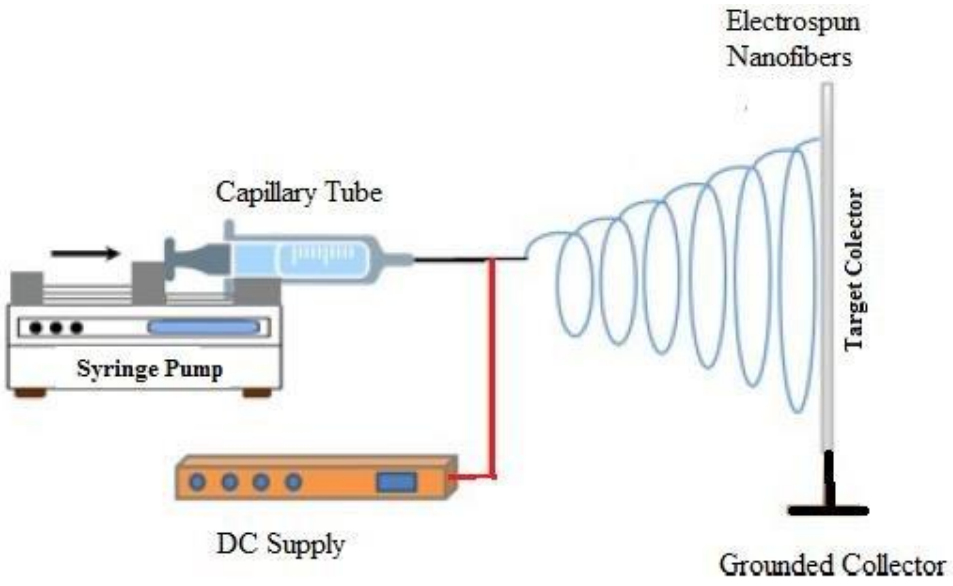

Figure 7. Representation electrospinning set-up

CHAPTER 2

MATERIALS & METHODS

2.1. Materials

PVDF (average molecular weight of 275,000, Sigma Aldrich), PEDOT:PSS (conductive grade, 1.3 wt. % dispersion in H_2O, Sigma Aldrich), PMMA (3 mm thickness) plate, were utilized for fabrication of photodetector. SCP Silver Conductive Paint was purchased from Assemcorp. Copper tape (12 mm x 16 m, 85 μm thickness), transparent double-sided adhesive (400 x 300 mm, 50 μm thickness, PET protecting layer copper clad plate laminate and pin heads purchased from local market. DMF (≥99.8%), deionized water and acetone were used to dissolve polymers. HNO_3 (≥65%, Sigma Aldrich), H_2SO_4 (Sigma Aldrich), HCl, (≥37, Sigma Aldrich) and NH_4OH (26%, Sigma Aldrich)) were for the functionalization of MWCNTs. Following light sources have been used for responsivity measurements; 850 nm (LED851L), 1200 nm (LED1200L), 1300 nm (LED1300L), 1450 nm (LED1450L), 1550 nm (LED1550L) and 1600 nm (LED1600L) LEDs supplied from Thorlabs and 405 nm, 465 nm, 525 nm and 625 power LEDs supplied from local market.

2.2. Fabrication of Conductive Network

Fabrication steps of the conductive network were explained below that explains how all the sensors were fabricated:

2.2.4. Preparation of PMMA substrate

PMMA substrates were prepared by Epilog Zing laser engraver (Figure 8(a)) via CorelDraw x8. 400 x 300 mm PMMA sheet was cut as described in the Table 1. The best result was obtained from specimen 11; therefore, all fabrication and measurement procedures in the following sections were performed with respect to this specimen. Vector cut settings were fixed to 30 % speed and 60 % power. Inner area was engraved 1 mm. Engraving settings were fixed to 20 % speed and 60 % power (Figure 8(b)). Prepared

PMMA substrates were functionalized with copper tape on each longer sides of the surface (Figure 8(c)).

Table 1. Physical properties of the PMMA substrates

Specimen	Outer frame (mm)	Inner frame (mm)	Vector cut	Engraved
1	20 x 12	12 x 4	✓	
2	20 x 12	12 x 8	✓	
3	41 x 8	16 x 2	✓	
4	10 x 5	6 x 0.833	✓	
5	10 x 6	6 x 2.4	✓	
6	20 x 6.4	5 x 2.4	✓	
7	10 x 10	8 x 6	✓	
8	10.8 x 7.2	6.8 x 3.2	✓	
9	10 x 5	6 x 1		✓
10	10 x 6.4	6 x 2.4		✓
11	10.8 x 7.2	6.8 x 3.2		✓

2.2.5. Electrospinning of PVDF

Partially align free-standing PVDF nanofibers was fabricated by electrospinning instrument (Figure 9(a)). 4.58 g PVDF was weighed in 20 ml vial and dissolved in 12 mL DMF and 3 mL Acetone to prepare 25 % wt. polymer dispersion. After a magnetic bar was put to the vial, dispersion was sealed and placed under stirrer. It was stirred for a day at 60 ^{o}C and 300 rpm. Following day, completely dissolved solution was transferred to 20 mL syringe and connected to the syringe pump in the electrospinning instrument. Collector of the instrument was coated with aluminum foil. Each PMMA substrate was prepared in the previous section was aligned on the middle of the collector with 2 cm distance. Up to 12 substrates were electrospun at once. The instrument parameters were as followed; 5 ml/h flow rate, 170 mm collector distance and 24 kV applied voltage. Besides, collector rotator was set to 500 rpm. Electrospinning process was performed for

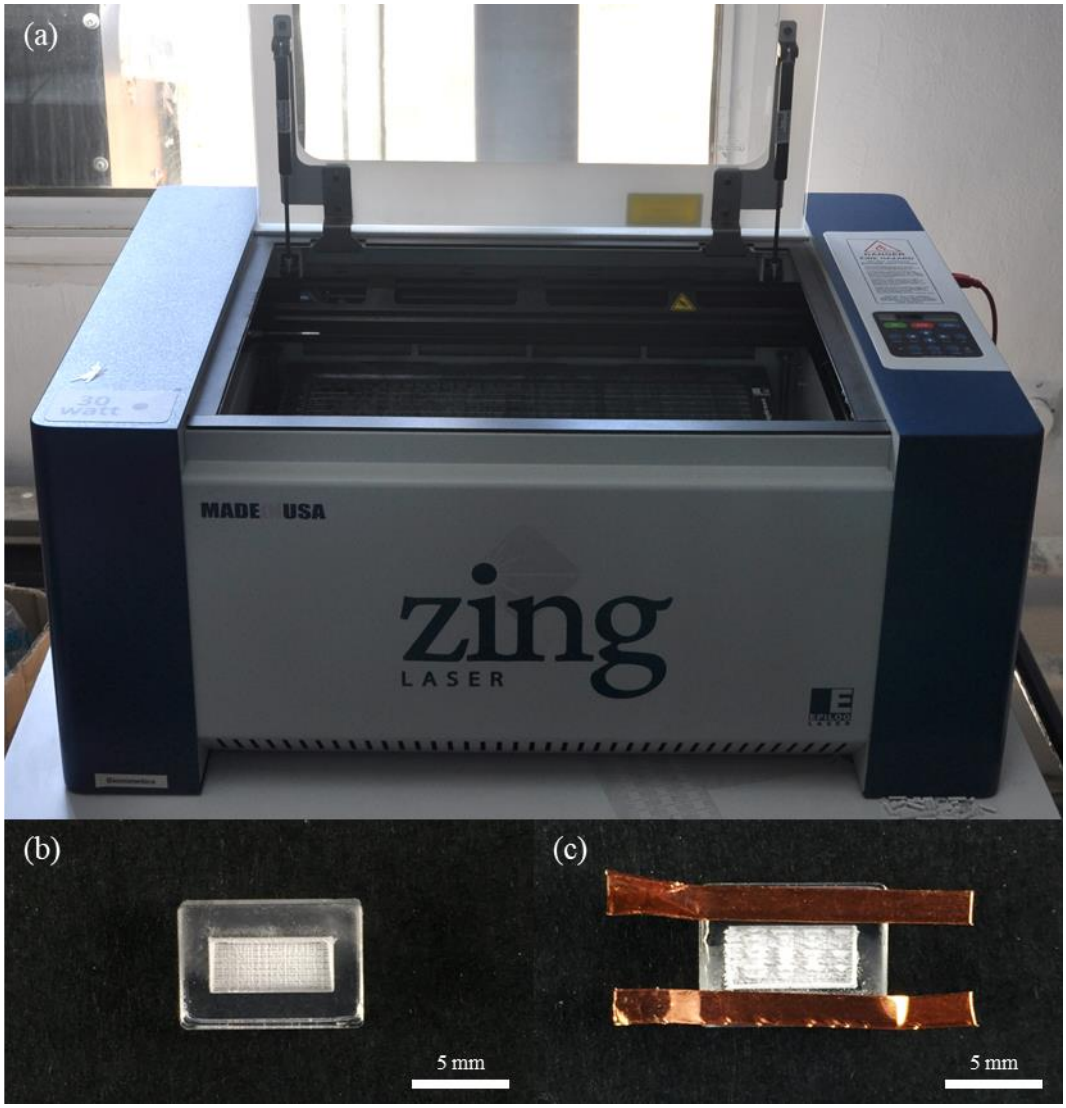

Figure 8. Digital image of (a) Epilog Zing laser engraver. Digital image of (b) bare and (c) copper tape functionalized PMMA substrates labeled 11 in the Table 1

two minutes for each set of devices. After PVDF electrospun through substrates (Figure 9(b)), they were removed from aluminum foil and stored in desiccator.

2.2.6. Acid Treatment of Carbon Nanotube

In 50 mL Erlenmeyer, 0.1 g MWCNT was weighed. Mixture prepared from 5 mL of H_2SO_4 and 1.7 mL HNO_3 was poured into the Erlenmeyer. Prepared mixture was sonicated for an hour and left in fume hood overnight. Afterward, 1.7 mL HCl was added to the solution and stirred gently. For neutralization process, 19 mL of NH_4OH was poured into mixture slowly. Additional NH_4OH might require until pH 7 was observed. Then, the mixture was filtered with cellulose acetate filter paper with 0.2 μm pore size.

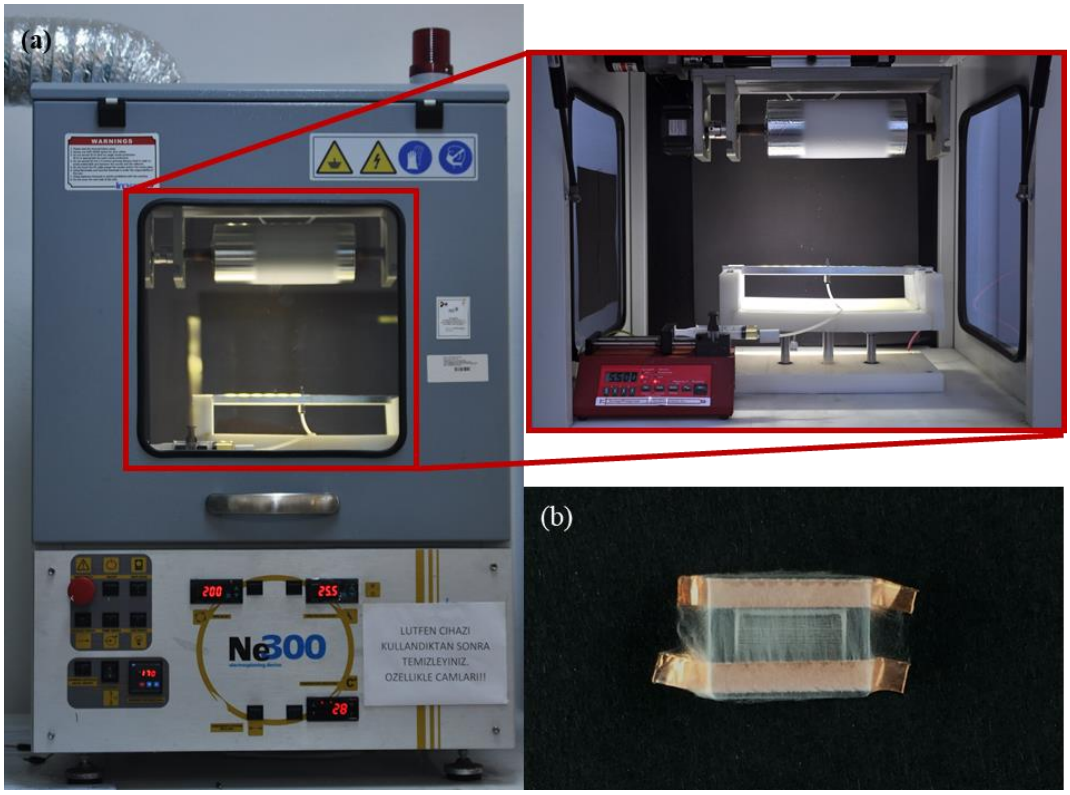

Figure 9. Digital image of (a) electrospinning instrument and (b) electrospun free-standing PVDF nanofibers

Filtrated product was taken to a 1 L Erlenmeyer and filled with deionized water until ca. pH 6 was observed. Finally, the mixture was filtered with the same procedure and dried in oven for three hours at 40 ^{o}C to obtain acid-treated MWCNT.

In order to prepare well-disperse MWCNT solution, acid-treated MWCNT granules were grinded in mortar. For 0.2 % wt. stock MWCNT solution, 20 mg was weighed in vial and 10 ml deionized water was added. Covered vial was put into sonicator for two hours and sonic homogenizer for 15 minutes with parameters as followed; 1 s on 9 second off pulse mode and 30 % power.

2.2.7. Surface Modification

Conductive materials were functionalized with drop-casting and spray-coating methods (Figure 10). For drop-casting technique, 1.3 % wt. PEDOT:PSS was diluted to 0.2 % wt., 0.1 % wt., 0.05 % wt., 0.02 % wt. and 0.01 % wt. with deionized water. 40 μL of PEDOT:PSS dispersion were drop-casted onto the middle of the free-standing PVDF nanofibers. Then, they were incubated in oven for an hour at 60 ^{o}C and 120 ^{o}C, respectively. Same procedure was applied for MWCNT dispersions except they kept in

oven for 2 hours at 50 ^{o}C. For spray-coating method, 0.1 % wt. PEDOT:PSS was prepared by diluting 1.3 % wt. stock to 0.5 % wt. with deionized water. Then, mid-stock was diluted to 0.1 % wt. with ethanol. 1 mL of prepared solution was transferred to tank of the spray coater and sprayed through the surface with ca. 20 cm distance. For all cases, silver conductive paste was applied above copper tape to make ohmic contact.

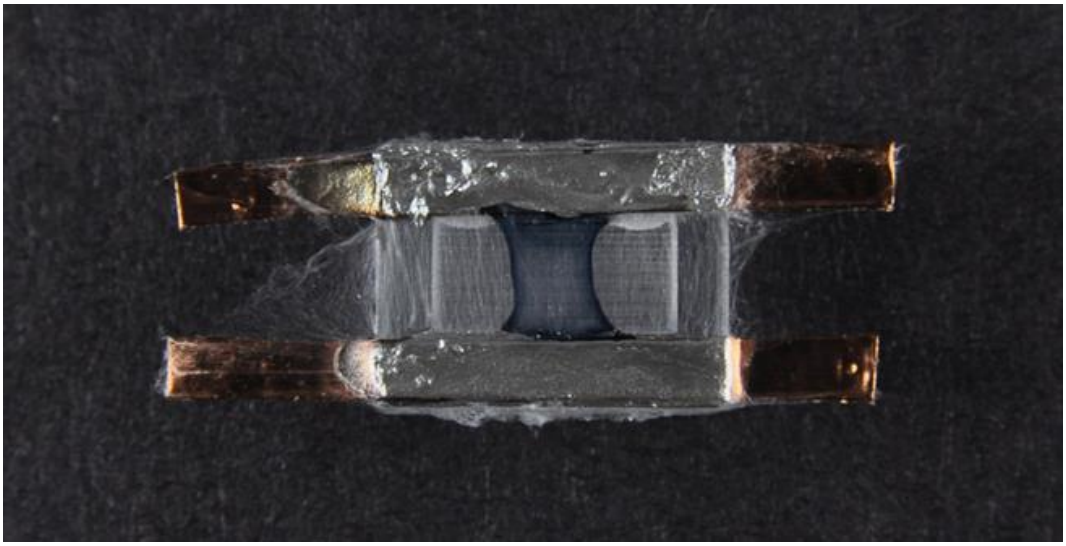

Figure 10. Digital image of PEDOT:PSS drop-casted specimen

2.2.8. Acid treatment of PEDOT:PSS

In order to enhance conductivity of the PEDOT:PSS based devices, PEDOT:PSS was treated with H_2SO_4 before silver conductive paste was applied. Pure H_2SO_4 was diluted to 1 M, 1.5 M and 2 M with deionized water. For drop-casted samples, 10 μL of solution was drop-casted onto the PEDOT:PSS surface and annealed at 120 ^{o}C for 30 minutes. After they were cooled down to room temperature, they were immersed to two beaker filled with deionized water, respectively, to remove residues. Finally, the devices were annealed again at 120 ^{o}C for 30 minutes. Same procedure was applied to obtain acid-treated spray-coated devices except 20 μL of acid solution was drop-casted onto the surface.

2.2.9. Printed Circuit Board Fabrication and Detector Mounting

PCB was fabricated to perform precise current measurements. Desired prototype was designed with Eagle 9.0.1 and printed to enamel paper (Figure 11). Bare copper clad

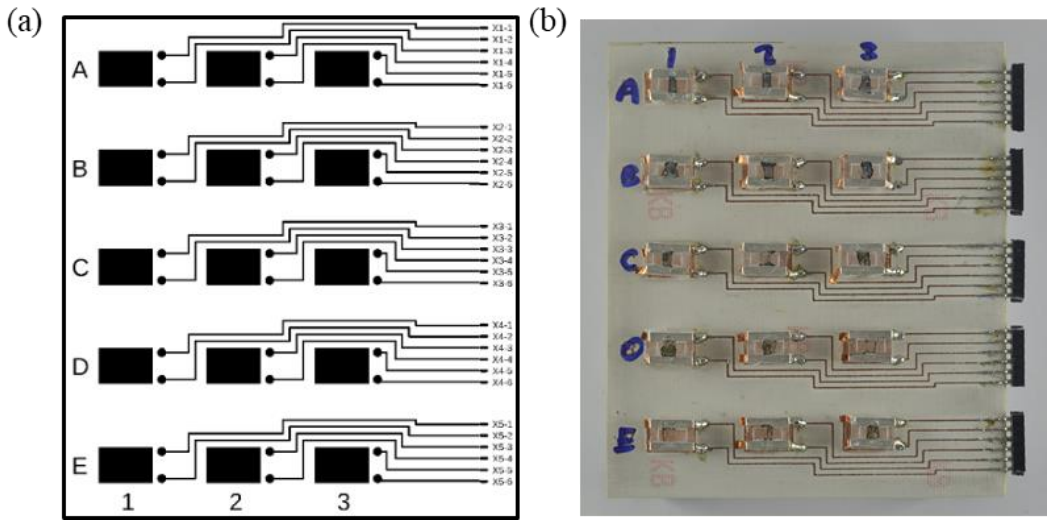

Figure 11. PCB design for photodetector array. Each array holds up 15 sensor which are connected to pins on the right side of the array

plate (95 x 110 mm) was cleaned with sandpaper and ethanol. Afterward, printed PCB design fixed backward to the copper side of the plate. By heating and applying pressure to the plate for 20 minutes, the ink on the paper transferred through the copper plate that provides protection during removal of copper from the surface. Ink printed paper was removed by gently rubbing under water. Then, the plate was immersed to the 20 mL of HCl : H_2O_2 solution (3:1). After complete removal of the copper from the surface was observed, PCB was cleaned with acetone and sandpaper to remove ink residues. Pin heads were fixed by soldering.

2.2.10. Fabrication of Bendable Photodetector

Bendable photodetector was fabricated on PET side of the double sided adhesive tape (Figure 12). While PMMA substrate was fabricated that mentioned in section 2.2.4, double sided adhesive was fixed between copper tape and PMMA substrate. Afterward, same procedures were followed as mentioned in earlier sections. After fabrication had been completed, PET substrate was taken off from PMMA surface. In the end, fully bendable sensor has been fabricated.

2.2.11. Scanning Electron Microscopy Analysis

Top view and cross section surface analyses were performed via SEM (Quanta FEG 250). Devices were fixed on a Carbon tape and coated with sputtered gold NP under

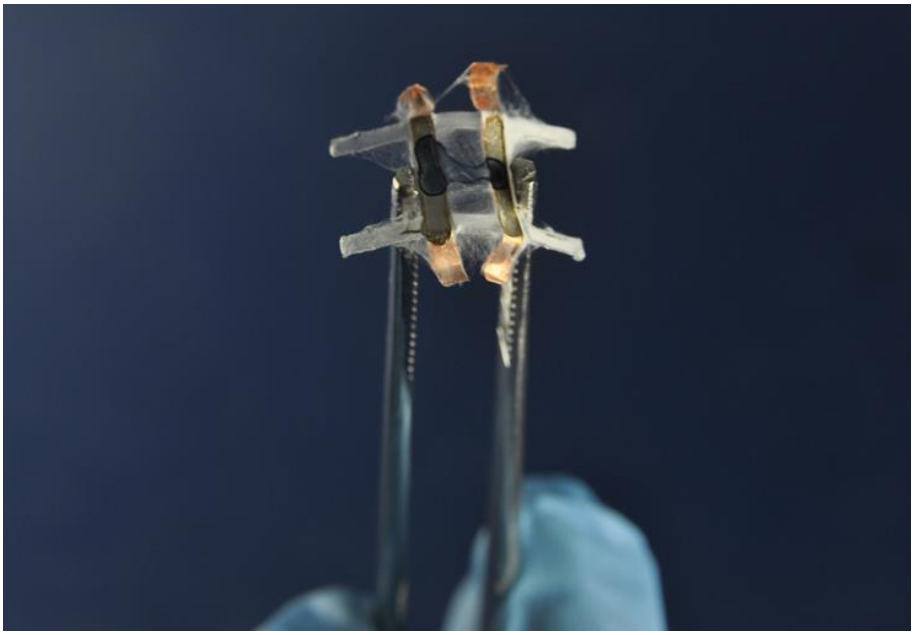

Figure 12. Digital image of bendable photodetector

Argon gas environment (Emitech K550X). Fiber diameters and conductive material thicknesses were calculated with Image J software (National Institutes of Health).

Figure 13. Digital image of SEM instrument

2.2.12. Atomic Force Microscopy analysis

AFM characterizations were performed by Nanosurf CoreAFM (Figure 14). Topography Force – Distance (F-d) curve measurements were carried out with Stad0.2LAuD static mod tip. On the other hand, ElectriMulti75-G tip was used

conductivity measurements. Topography measurements were edited with Scanning Probe Image Processor (SPIP) and Gwyddion software. F-d curves analysis were performed with AtomicJ software (Hermanowicz, Sarna, Burda, & Gabryś, 2014).

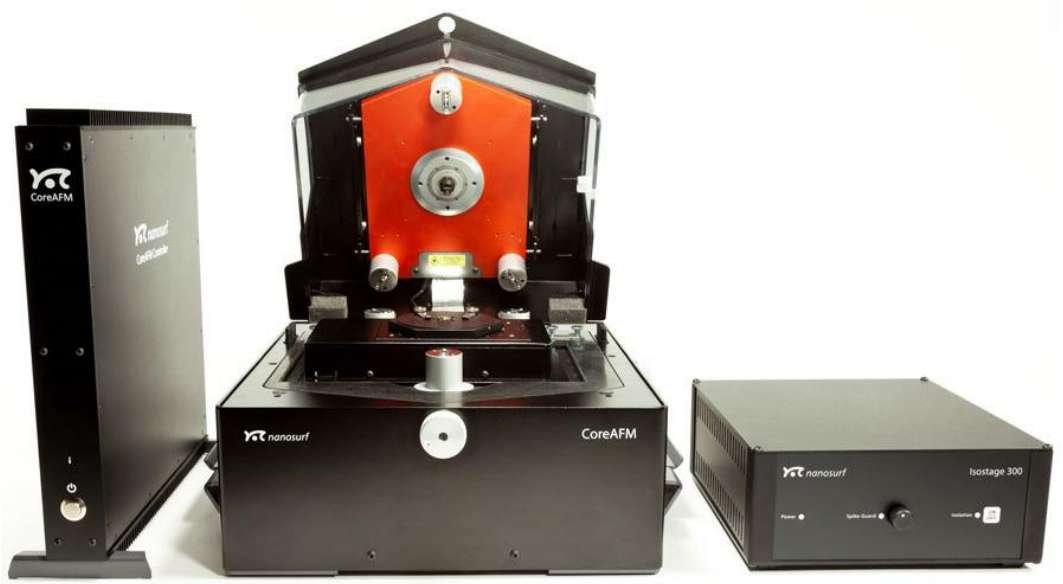

Figure 14. Digital image of Nanosurf CoreAFM

2.2.13. Electrical Characterization

DC measurements were carried out with HP 4145B Semiconductor Parameter Analyzer and HP 34401A Digital Multimeter (Figure 15)**.** The fabricated photodetector devices were connected to copper pads by soldering. Measurements were performed by connecting to multimeter or semiconductor parameter analyzer via two pins. IV measurements were performed with multimeter by adjusting DC power supply manually sweep from 0 V to 5 V with 0.2 V intervals. Responsivity measurements were carried out with 1 V constant bias. Photodetectors were illuminated with light sources starting from IR LEDs (850 nm, 1200 nm, 1300 nm, 1450 nm, 1550 nm and 1600 nm, Thorlabs) and followed by 625 nm, 525 nm, 465 nm and 405 nm LEDs, respectively. Each illumination was performed with 5 replications and their average with standard deviation has been considered while calculating responsivity. VOC responsivities were measured by exposing given amount of VOCs intermittently through the gas chamber.

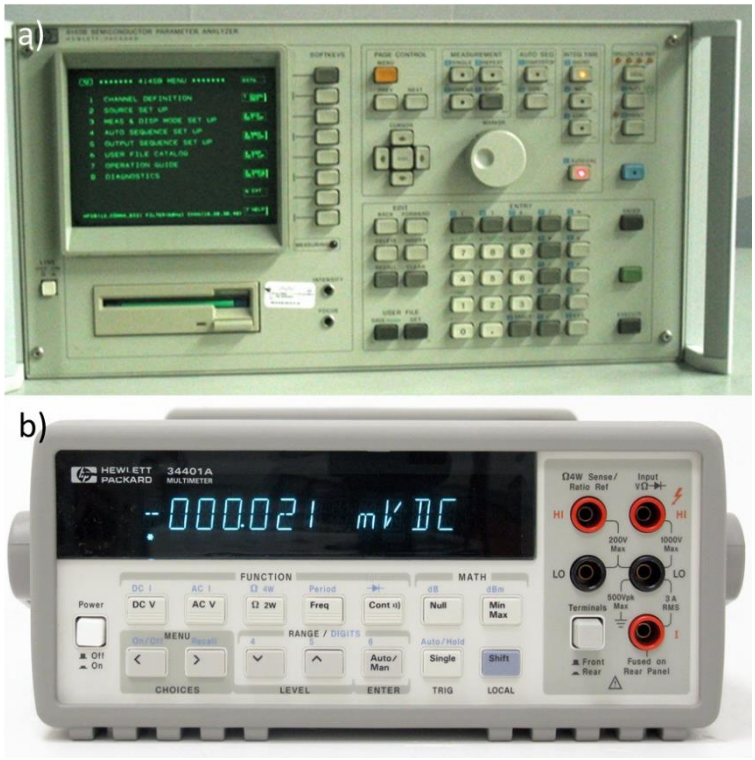

Figure 15. Digital image of (a) HP4145B Semiconductor Parameter Analyzer and (b) HP34401A Digital Multimeter

CHAPTER 3

RESULT & DISCUSSION

3.1. Conductive Network Characterization

Conductive network was prepared as represented in Chapter 2. Fabricated sensors were characterized as described below:

3.1.1. PVDF nanofiber Characterization

Solid PMMA substrates were prepared as defined in earlier section. According to process, PMMA substrates were cut to frame like shape. In order to electrospun free-standing align PVDF nanofibers, there should be an air gap between electrodes. That air gap influences the electric field flows from syringe through the collector of electrospinning instrument. Therefore, all specimens have air gap in the middle produced by either engraved or cut. It was observed that engraved ones were exhibited better alignment during electrospinning as engraved area blocks the electric field from syringe to collector itself.

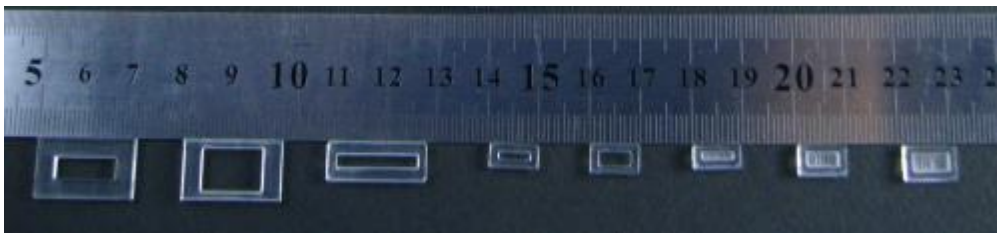

Figure 16. Digital image of fabricated PMMA substrates

3.1.2. Surface Characterization of PVDF Nanofibers

PVDF nanofibers were fabricated with electrospinning technique. Figure 17 depicts the SEM images of the PVDF nanofibers. It was clear that free-standing PVDF nanofibers (Figure 17a) were tend towards to the poles of the devices. On the other hand, PVDF nanofibers were oriented randomly on the conductive copper surface of the device.

This phenomena observed due to the manipulation of electric field. Such that, copper tapes on each pole attract to electric field themselves and this distraction causes nanofibers to stretch and attach to the copper tapes on the substrate.

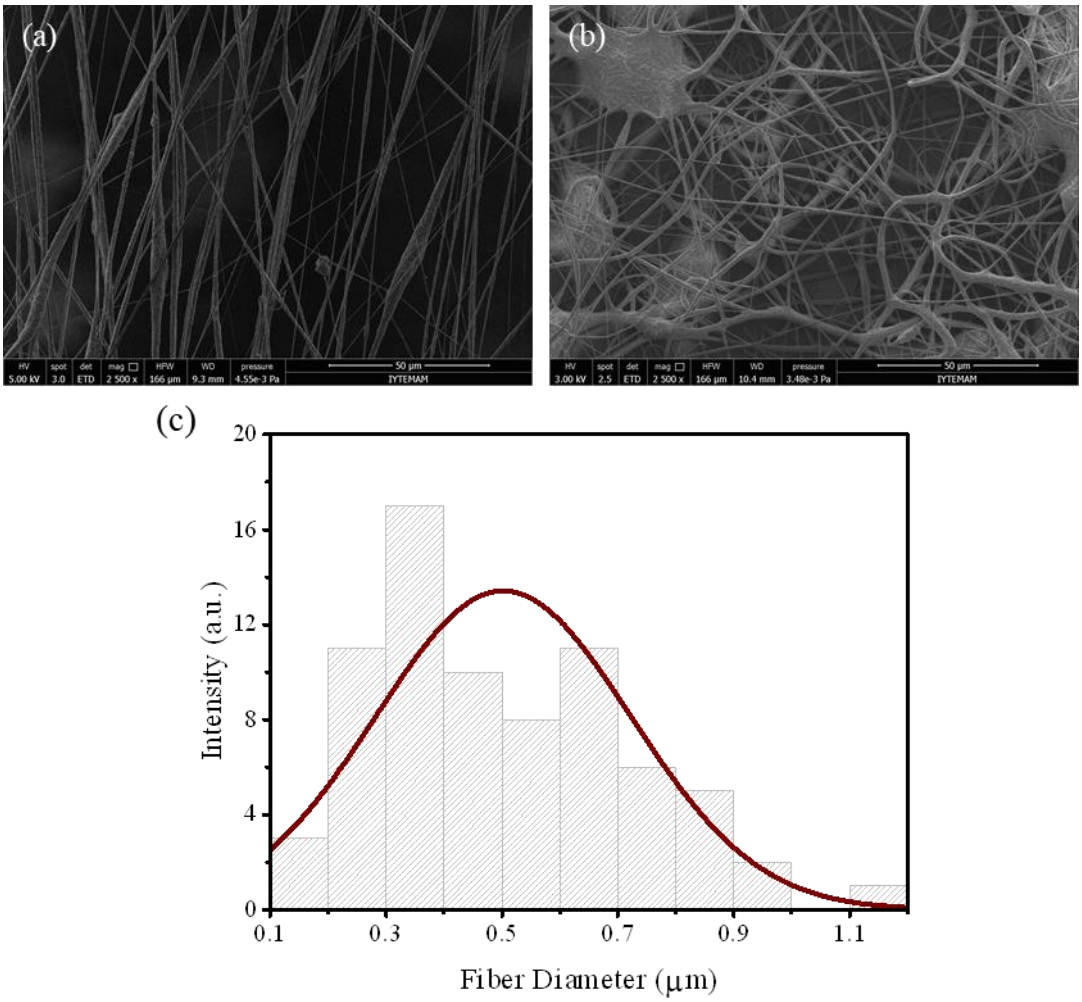

Figure 17. SEM images of PVDF nanofibers (a) between poles and (b) on the copper surface electrospunned through specimen 11. Distribution of free-standing fiber diameter. Average fiber diameter was calculated as 447 nm

3.1.3. Surface Characterization of PEDOT:PSS Based Sensors

Electrospunned PVDF nanofibers were functionalized with PEDOT:PSS by drop casting and spray coating technique. Figure 18 illustrates the SEM images of the free-standing PEDOT:PSS functionalized devices fabricated by drop-casting (Figure 18(a, b)) and spray coating (Figure 18(c, d)) techniques. Functionalization of the flexible substrate via drop-casting technique resulted in a formation of homogeneous film

comprised of PEDOT. On the other hand, PSS was observed to be crystallized on the surface while incubation. Thickness of the PEDOT:PSS layer was calculated as ca. 477 nm. On the other hand, when substrate was functionalized with spray-coating technique, PEDOT was coated the free-standing PVDF nanofibers. Albeit, micrometer scale PEDOT films were observed (Figure 18(c, d)) like domains. As the whole network considered, they just look like a neurons and synapses communicating each other.

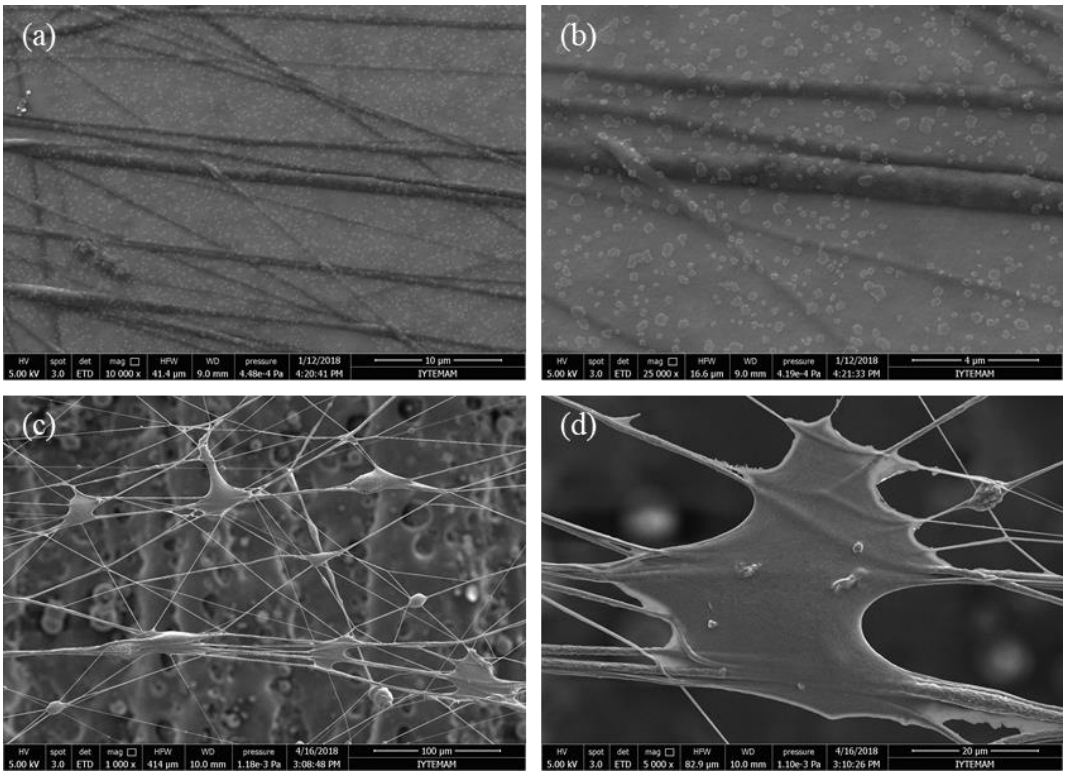

Figure 18. SEM images of PEDOT:PSS (a, b) drop casted and (c, d) spray coated PEDOT:PSS device

Figure 19 depicted the AFM analysis of the device fabricated by drop-casting PEDOT:PSS. It illustrated that PEDOT formed a film like structure and spread on to the PVDF nanofibers homogenously. Besides, PSS salt were observed on the surface with a flake liked shape. PSS flakes are generally flat; however, some of them have a bulging out in the center or have a depression in the center. Average roughness of the PEDOT:PSS was calculated as 50 nm. Typical F-d curve of the sample was illustrated in Figure 19(d). Young's Modulus of the sample was calculated as 21.5 MPa.

In order to perform the AFM analysis, Stad0.2LAuD AFM tip was used in static force modulation mod. Set point was set to 20 nN. However, it may need to be increased for better tip-surface interaction. P-I-D gains were set to 300, 800 and 200, respectively

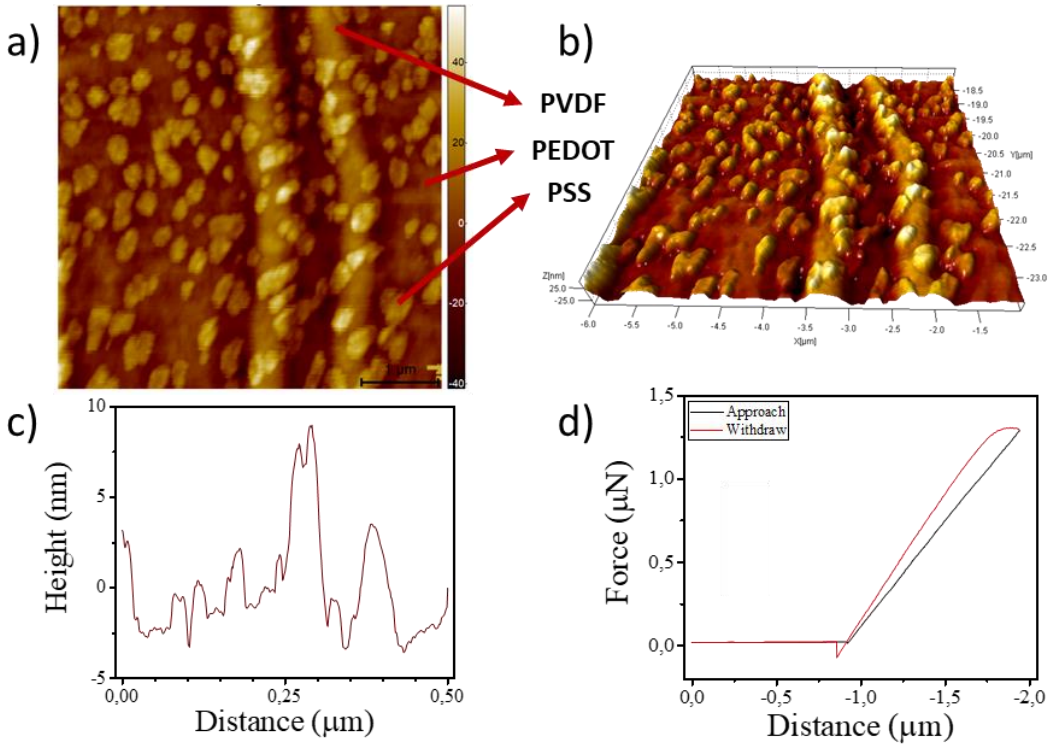

Figure 19. (a) 2D and (b) 3D AFM topography of Free-Standing PVDF-PEDOT:PSS network. (c) cross-section and (d) F-d analysis of the specimen that Young's Modulus was calculated as 21.5 MPa

where P gain used to overlap forward and backward lines, I gain increases the surface-tip interaction while increasing deflection noise and D gain decreases the deflection noise while increasing smoothness of the measurement. F-d analysis was performed by setting start offset -500 nm and range 1 µm. Modulation time was set to 1 second while collecting 1024 data points. After the measurement has been performed, AtomicJ software was used to analyze the F-d curves. Processing Assistant setting was adjusted as follow;

- Contact Estimator : Classical Golden
- Estimation Method : Model Independent
- Model : Sphere (Hertz)
- Radius : 0.007 µm
- Poisson Ratio : 0.5

- Calibration : Read-in option was checked
  Rest of the settings were left as default.

3.1.4. Surface Characterization of MWCNT Based Sensors

Free-standing PVDF nanofibers were functionalized with MWCNTs, as well. Figure 20 illustrates the SEM images of the devices functionalized with MWCNT via drop-casting technique. Just like PEDOT, MWCNTs formed a homogeneous film on the surface by entangled together. Observable cracks with various sizes in MWCNT network were naturally occurred defects on the surface. Penetration of MWCNT into the PVDF surface forms an uneven distribution of the network and rough morphology resulted in higher amount and larger sized of crack. On the other hand, paper-like morphology of PVDF substrate soften the surface that reduce the formation of cracks.

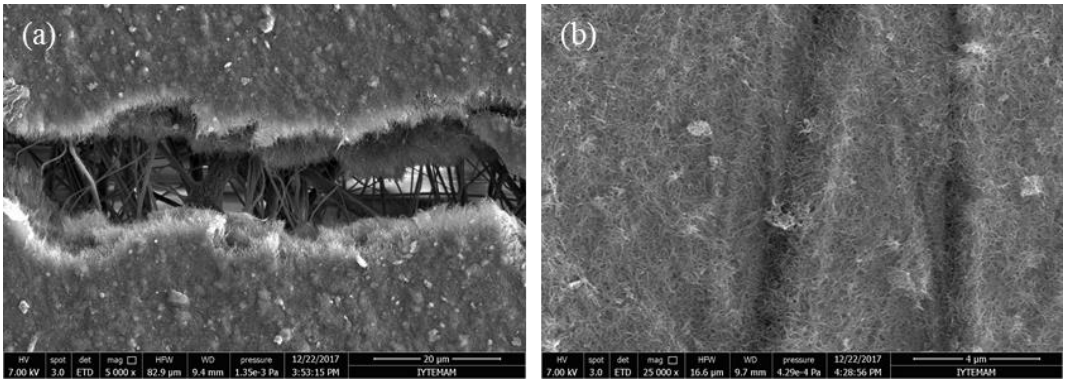

Figure 20. SEM images of the MWCNT drop casted device

Figure 21 illustrates the AFM analysis of the device fabricated by drop-casting MWCNT. AFM image show that MWCNTs spread all over the surface homogeneously such that they even cover the PVDF nanofibers. Surface roughness was calculated as 400 nm. F-d analysis in Figure 21(d) was performed by penetrating AFM tip 1 μm. Average Young's Modulus was calculated as 909.4 MPa which was due to the more brittle nature of MWCNT.

3.1.5. Surface Characterization of MWCNT Percolated PEDOT:PSS Based Sensors

PEDOT:PSS dispersion was percolated with MWCNT to enhance the devices conductivity. Figure 22 represented the SEM images of the PEDOT:PSS-MWCNT

network fabricated by percolating PEDOT:PSS dispersion with MWCNT. After deposition and incubation, PEDOT conserve its homogeneity and disperse all over the active region; however, MWCNT formed their own domains and stay together.

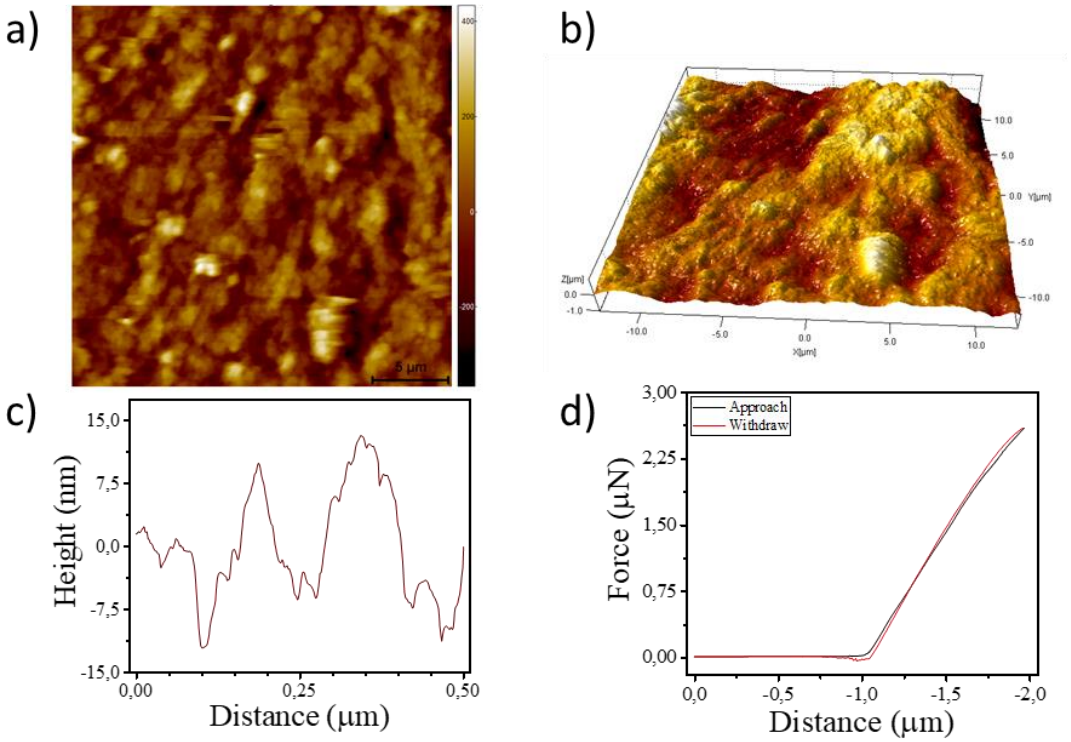

Figure 21. (a) 2D and (b) 3D AFM topography of Free-Standing PVDF-MWCNT network. (c) cross-section and (d) F-d analysis of the specimen that Young's Modulus was calculated as 909.4 MPa

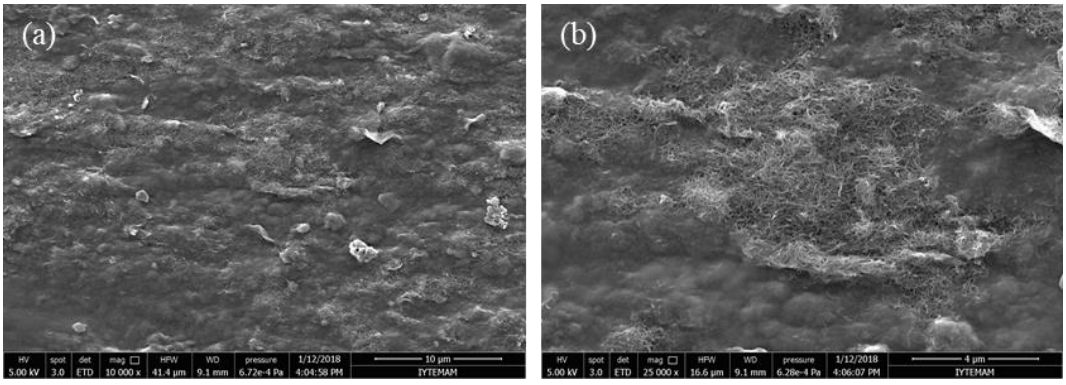

Figure 22. SEM images of the MWCNT percolated PEDOT:PSS based device

3.1.6. Surface Characterization of ZnO doped PEDOT:PSS Based Sensors

In order to alter responsive region of the PEDOT based device, fabricated sensors were doped with ZnO nanoparticles. Figure 23 depicted the SEM images of ZnO doped PEDOT:PSS based device. As shown in Figure 23a, ZnO nanorods were distributed partially homogeneously all over the surface yet incontrovertibly ZnO domains formed. Figure 23b shows closer view to ZnO domains.

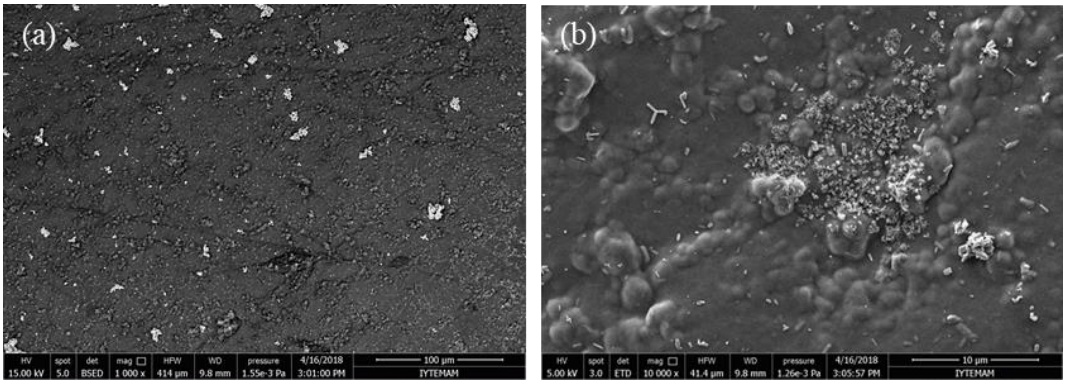

Figure 23. SEM images of the ZnO doped PEDOT:PSS based device

3.1.7. Surface Characterization of Acid Treated PEDOT:PSS Based Sensors

PEDOT:PSS based devices treated with sulfuric acid solution to enhance conductivity. Figure 24(a, b) illustrates the acid treated PEDOT:PSS devices fabricated by drop-casting technique. Albeit acid treatment did not affect homogeneity of the film surface and formed any crack, circular shaped deformations formed after treatment which may due to the sulfuric acid that remains on the surface during first incubation while water was evaporated.

3.2. Fabrication of Polymer Nanofiber-Conducting Polymer Fabric and Noncontact Motion Sensing Platform

Low-cost and low-power indoor localization or tracking infrared sensors have attraction in market and scientific community for location-based products like automatic lighting or heating switches. Furthermore, occasionally, high accuracy is beside the point.

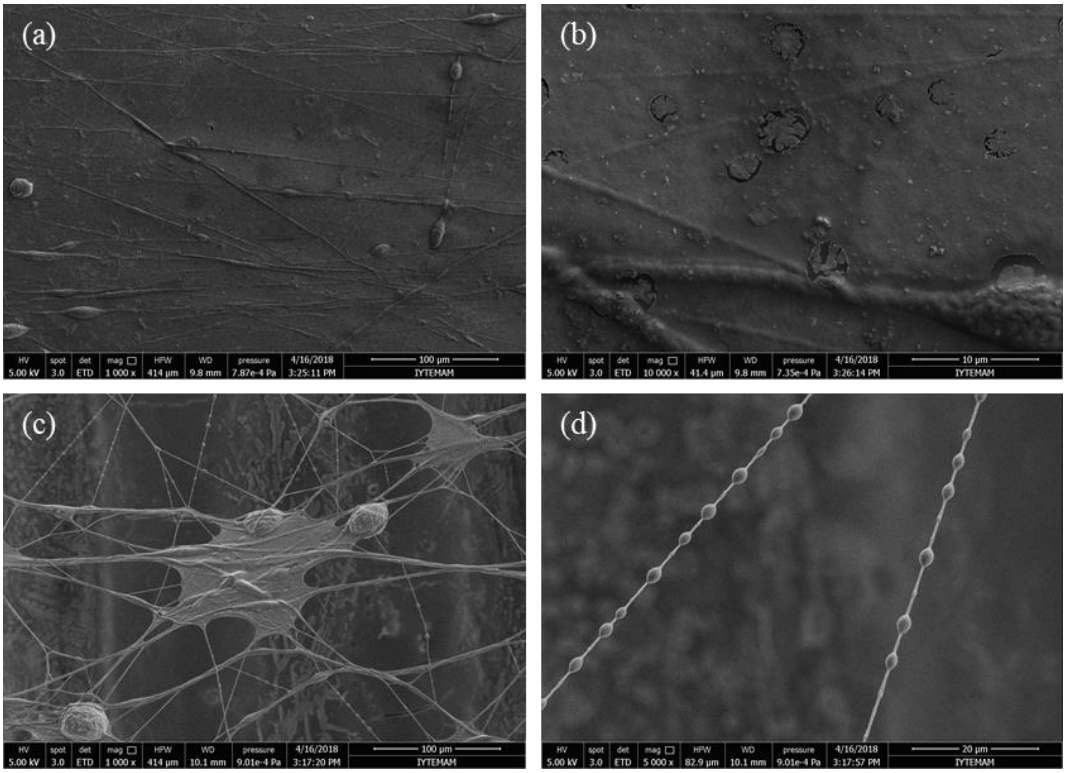

Figure 24. SEM images of the acid treated (a, b) drop casted and (c, d) spray coated PEDOT:PSS device

For example, following an elder human alone in the living space which can detect unusual activities e.g. oversleeping or staying in a space more than usual that may due to a disease or heart attack. On the other hand, the other method that measures the electrical field change affected by conductive objects is capacitive sensors. A well-known example is the Theremin instrument that can be controlled touchless with two bare hands. Measuring dielectric forces of human tissues were always carrying a great importance in sensor development and physiological sciences. In the past, dielectric properties of human tissues were measured in variety of frequency range. However, we suggest a novel noninvasive measurement technique that can detect proximity without any radiation sources. Here we explained that combination of conductive polymer-electrospun polymer nanofiber network to host iron oxide nanoparticles providing micrometer thick sensing interface. The sensor has fabricated as free-standing fabric exhibiting 10 to 100 kOhm base resistivity upon bias applied. The moving object has been sensed through the electrostatic interactions between fibers and object. By the controlled combination of conductive polymers electrospun polymer nanofibers effective device miniaturization has

been provided without loss of performance. The noncontact motion sensor platform has unique flexibility and light weight holding a potential for wearable sensor technology.

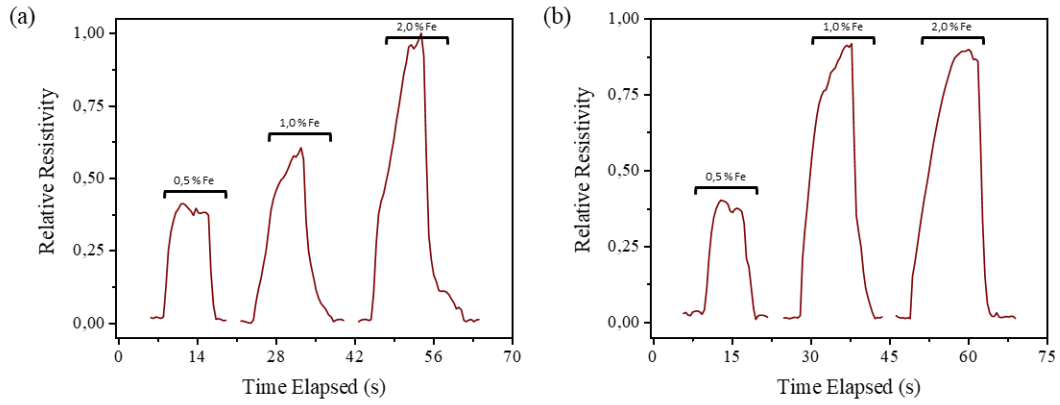

Figure 25. Relative resistivity measurement over time of 0.05 %, 0.1 % and 0.2 %FeNP doped (a) PEDOT:PSS-PVDF and (b) CNT-PVDF nanofiber network to human finger

Measuring dielectric forces of human tissues were always carrying a great importance in sensor development. Combination of conductive polymer – PVDF nanofiber network to host iron oxide nanoparticles providing micrometer thick sensing interface. Figure 25 shows that both PEDOT:PSS and CNT drop cast sensors work well when exposure to dielectric force. In Figure 25(a), PEDOT:PSS-PVDF network, doping FeNP beyond 0.1% causes saturation, on the other hand; MWCNT-PVDF network (Figure 25(b)), linear increment without saturation was observed. The moving object has been sensed through the electrostatic interactions between fibers and object. The sensing range was found to be 1-5 cm from sensor interface referring to electrostatic interaction range of human finger and surface is traceable distance for wearable fabric technology. The signal reproducibility was 95 % for hundred trials assuring the reusability of sensor. The sensor response exhibit variation substantially among ten volunteers. This result confirms that finger electrostatic extent is person specific and the sensor platform response to the variation.

3.3. Polymer Nanofiber-Conductive Layer based Photoresistive Network Generating Circuits

Fabricated devices were utilized for photoresistive network which were respon-

sive from UV to NIR region.

3.3.1. Electrical Characterization of PEDOT:PSS Based Sensors

Electronic features of the fabricated devices were investigated by drop-casting different concentration of PEDOT:PSS through the free-standing PVDF nanofibers. Figure 26(a) shows the average resistivity of the PEDOT:PSS based devices fabricated by drop-casting 40 μL of 0.01 %, 0.02 %, 0.05 %, 0.1 % and 0.2 % (wt.) PEDOT:PSS dispersion respectively. Highest resistivity was observed as circa 170 KOhm. Base resistivity was as low as 10 KOhm with the increasement of PEDOT:PSS concentration. It was obvious that deviation from average resistivity was decreased dramatically with the increasement of concentration of PEDOT:PSS dispersion. This feature was observed due to the fact that the thickness of the PEDOT:PSS layer would be thinner with the decrement of the concentration. On the other hand, there was no significant change in the average resistivity beyond the concentration of 0.1 % as the thickness of PEDOT:PSS would be enough to carry the applied 5 V bias. For that purpose, J-V curves of the corresponding devices were investigated in Figure 26(b). Even though there were no significant change in the resistivity of the devices, J-V curves were visa-versa.

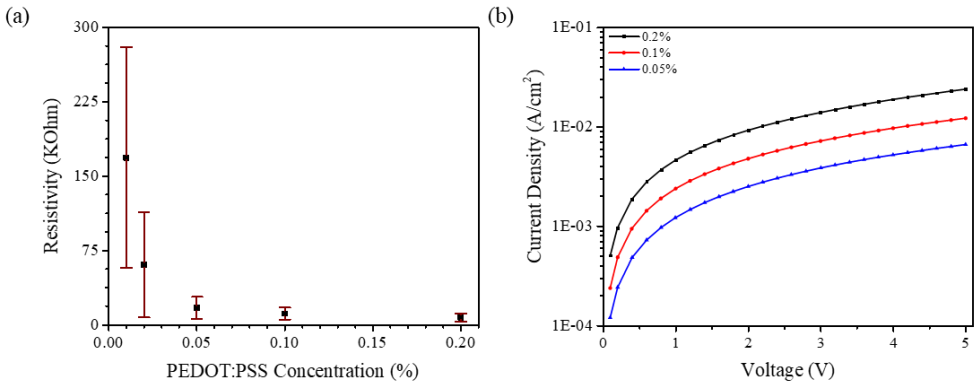

Figure 26. (a) Effect of the PEDOT:PSS concentration to the resistivity fabricated by drop-casting 40 mL of 0.01 %, 0.0 2%, 0.05 %, 0.1 % and 0.2 % PEDOT:PSS dispersion respectively. (b) Current Density of the PEDOT:PSS based drop-casted devices

Photo sensing capability of the devices were investigated by illuminating with light sources in the range from UV to NIR region. Figure 27(a) illustrates the Responsivity of the PEDOT:PSS based devices under illumination with 10 different light sources

(405 nm, 465 nm, 525 nm, 625 nm, 850 nm, 1200 nm, 1300 nm, 1450 nm, 1550 nm and 1600 nm). According to this, responsivity of the devices was directly proportional to the concentration of PEDOT:PSS dispersion. It shows dramatic response to the light sources. The most responsive point was observed by illuminating with 625 nm. Besides, there was no significant responsivity difference in the near IR region. On the other hand, when spectral response of the device that contains 0.2 % PEDOT:PSS dispersion, which was the most responsive device among others, was investigated, Figure 27(b), the device was relatively produce more photocurrent density illuminated with near IR light sources. The most photocurrent production was obtained by illuminating with 405 nm and 850 nm light sources. Their response times were calculated as 1250 ms and 1320 ms, respectively.

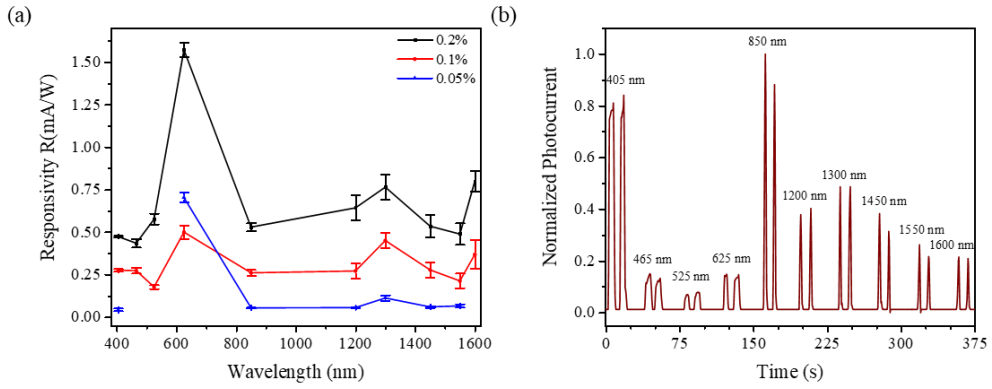

Figure 27. (a) Responsivity of the PEDOT:PSS based devices. (b) Spectral response of 0.2% PEDOT based device from UV to NIR region

Electrical characteristic of the device was studied with AFM, as well. Figure 28 shows the IV curves taken from the green points represented insets of the graphs. Figure 28 illustrates the topography of the device and IV curves taken from green dots as shown in their inlets and . Figure 28(b) and Figure 28(c) were represented IV curves taken from the point where PVDF nanofibers rest and the PEDOT film formation observed. Comparison of two IV curves revealed the fact that majority part of the current transmission was observed around the PVDF fibers which have not hitherto been investigated.

3.3.2. Electrical Characterization of MWCNT Based Sensors

In order the investigate the effect of the MWCNT amount, photo-resistor devices were fabricated in different concentrations. Figure 29(a) illustrates the variation of resis-

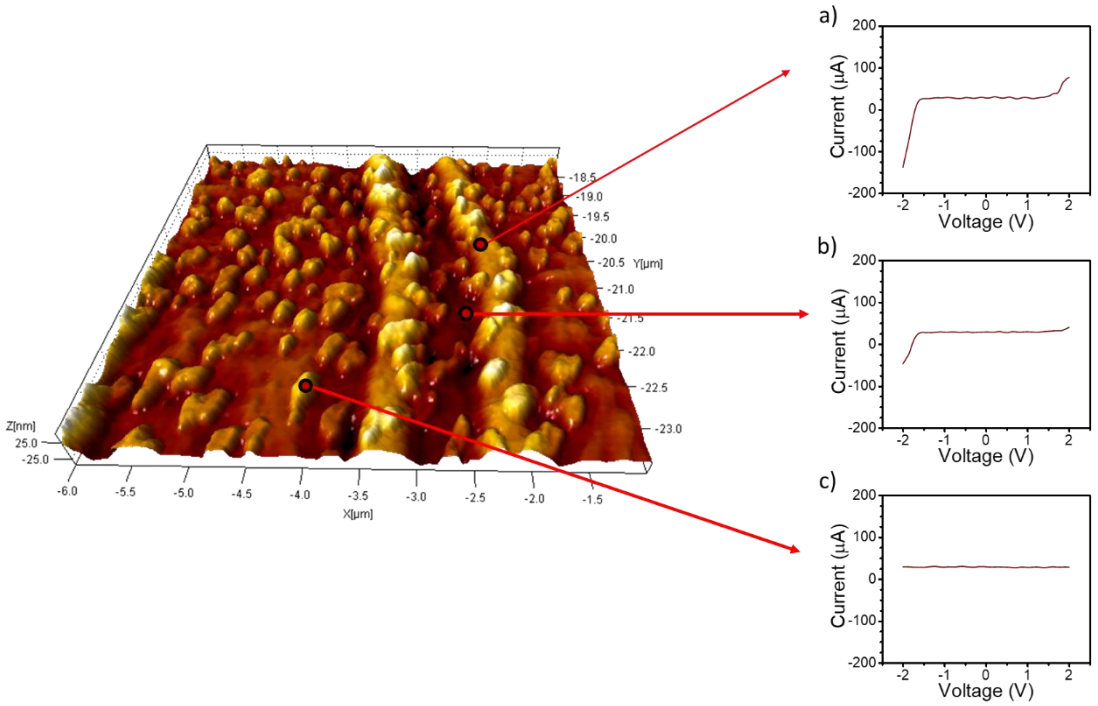

Figure 28. AFM topography and IV curves of drop-casted PEDOT:PSS based device measured from (a) PEDOT from fiber (b) PEDOT from film and (c) from PSS region of the surface

tivity with respect to the MWCNT concentration fabricated by drop-casting 40 μL of 0.01 %, 0.02 %, 0.05 %, 0.1 % and 0.2 % (wt.) MWCNT dispersion. The base resistivities were 9.62 ± 0.48, 3.02 ± 0.15, 1,08 ± 0.05, 0.50 ± 0.02 and 0.22 ± 0.01 for the MWCNT concentrations; 0.01%, 0.02%, 0.05%, 0.1% and 0.2%, respectively. Lower MWCNT concentrations disrupt the homogeneity of the MWCNT network that causes disorder in base resistivity. On the other hand, higher MWCNT concentration offers more stable structure that resemble each other. Figure 29(b) plots the typical J-V curve of the Ag-MWCNT-Ag sandwich type ohmic interaction from 0 V to 4 V in different MWCNT concentrations in dark current. Photo-resistors show symmetric behavior under reverse bias as expected due to the lack of another junction(s). Additionally, Ag and MWCNT exhibit excellent harmony above hanging PVDF substrate which increases the surface area of the MWCNT because of the cavity in the middle.

Characteristics of broadband photoresponse of photo-resistors as a function of incident wavelength is investigated by using LEDs from UV to infrared range. Figure 30(a) plots the responsivities in the range from 400-1600 nm which can be observed clearly that photo-resistors have a broadband responsivity by applying a 1 V bias since

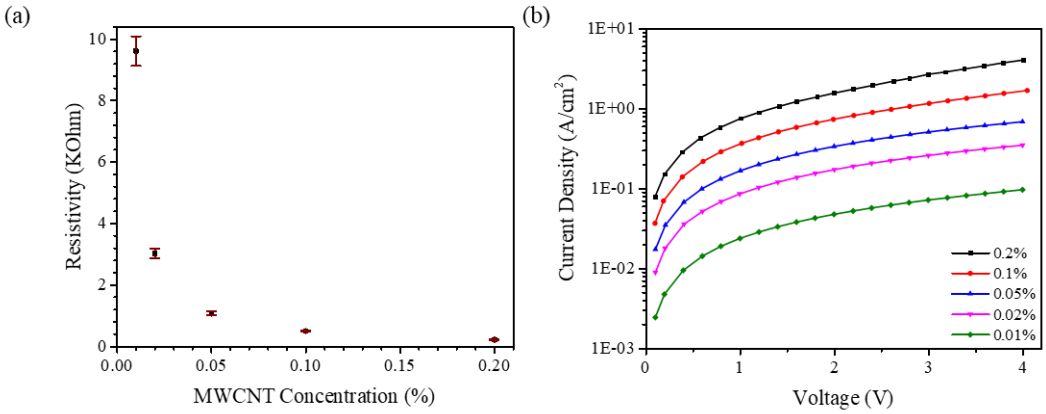

Figure 29. (a) Effect of the MWCNT concentration to the base resistivity fabricated by drop-casting 40 μL of 0.01 %, 0.02%, 0.05 %, 0.1 % and 0.2 % MWCNT dispersion. (b) Typical room temperature J-V curves of the photo-resistors in dark current

the increasement of bias voltage causes in fluctuations even amplify the obtained photocurrent significantly (Figure 32). As observed in Figure 30(b), photo-resistors have linearity in the infrared region on the contrary of the increasement in the wavelength of incident light. Surprisingly, 0.1% MWCNT contained photo-resistor have higher responsivity than the one contains 0.2% MWCNT almost all incident wavelengths, which was showed particularly in Figure 30(a) that illustrates the photocurrents of the photo-resistors in various MWCNT concentration illuminated by 850 nm light source with intensity of 25.9 mW/cm^2. The origin for this phenomenon is still unknown and needs further investigation.

The below (Figure 30(a)) photoresponses implies that 0.1% MWCNT contained photo-resistor would be the best choice, due to the highest responsivity among others, used as a low-consumption device that able to detect irradiation in both visible and near infrared region. For that reason, photoresponse of the 0.1% MWCNT contained photo-resistor investigated in detail. Figure 30(b) depict the photoresponse of the corresponding photo-resistor under pulsed illumination with different wavelengths in both visible and infrared regions. Significantly, at an applied bias voltage of 1.0 V, the current increased 7.69 μA and further to 15.8 μA with the illumination by 525 nm and 405 nm light sources, respectively.

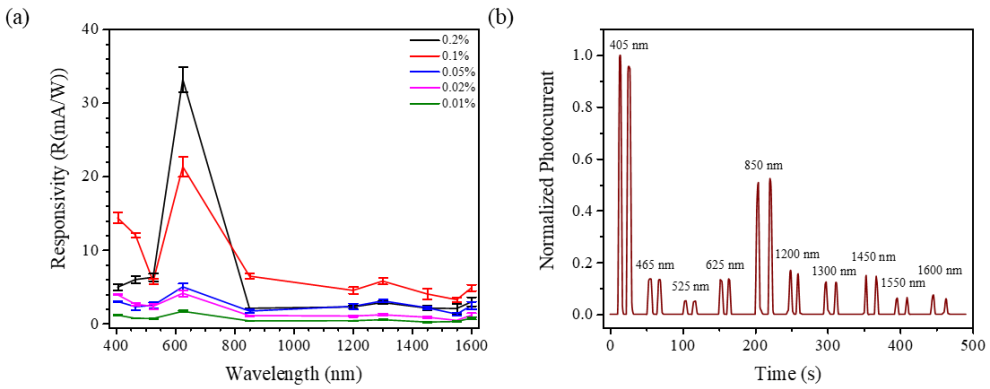

Figure 30. (a) Responsivity of the MWCNT based devices. (b) Spectral response of 0.2% MWCNT based device from UV to NIR region

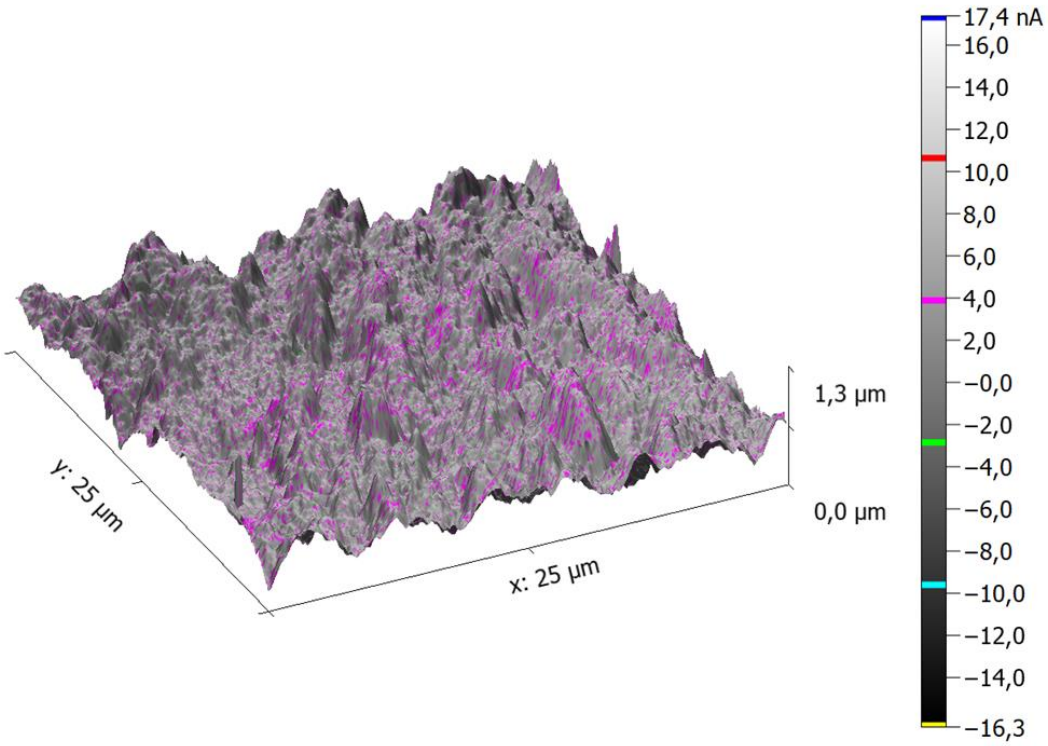

Figure 31. Conductive mapping of 0.2% MWCNT based sensor

3.3.3. Electrical Characterization of MWCNT Percolated PEDOT:PSS Based Sensors

In order to alter the photoresponsivity of the devices MWCNT based devices were percolated with PEDOT:PSS. Figure 33(a) illustrates the resistivity distribution of the devices as a function of percolation rate (0 %, 25 %, 50 %, 75 % and 100 % (v/v)). The results showed that MWCNT was predominant with respect to resistivity though the copious amount of PEDOT:PSS since there was no significant current density variation among 50 %, 75 % and 100 % MWCNT based devices with respect to Figure 33(b). The reason is, due to the one order of magnitude conductivity difference, electrons would rather going along to the more conductive path composed of MWCNT because SEM images (Figure 22) showed that MWCNTs have their own networks all over the active layer however; PEDOT conserve it homogeneity on the surface.

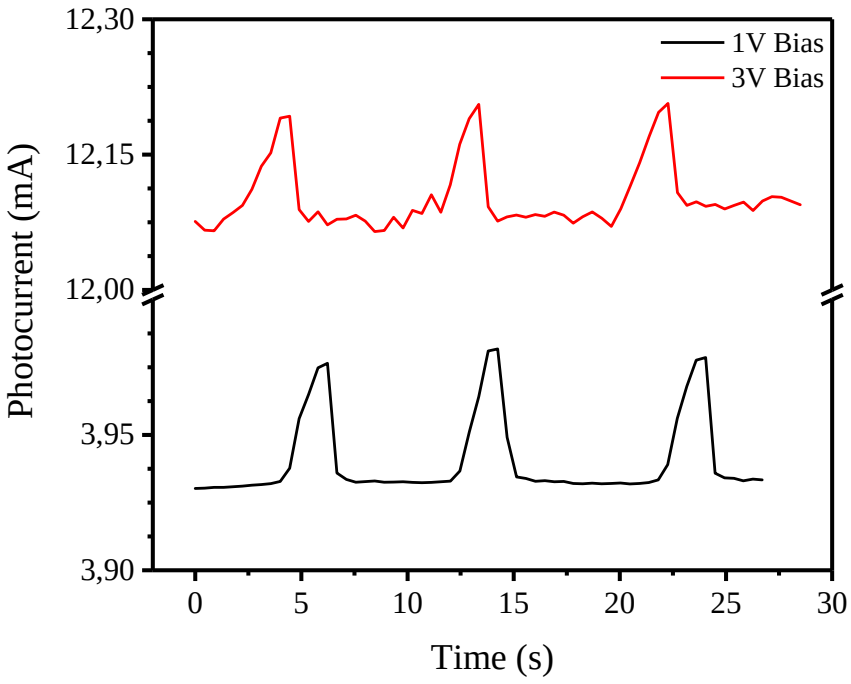

Figure 32. Photocurrent change of 0.2% MWCNT device under illumination with 850 nm light source upon applied bias at 1 V (black) and 3 V (red)

Photo responsivity of the percolated devices were studied, as well. Figure 34(a) depicts the responsivity of the percolated devices. There were two distinct difference between PEDOT:PSS and MWCNT based devices. One was the responsivity at 1300 nm

and at 525 nm. For 50 % and 75 % percolated device, the responsivity at 525 nm was depressed and at 1300 nm was boosted. This alteration was observed resulted in the interaction of two conjugated materials at particular ratio.

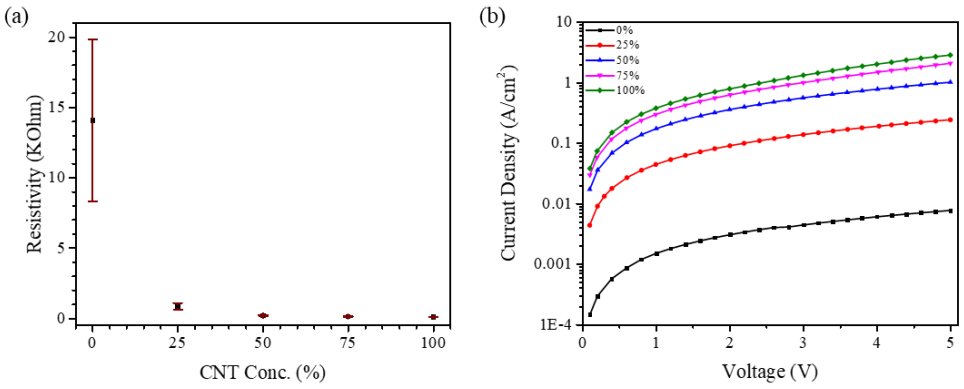

Figure 33. (a) Distribution of resistivity resulted in percolation of MWCNT with PEDOT:PSS with a rate of 0%, 25%, 50% 75% and 100% (v/v) and (b) J-V curves of represented devices

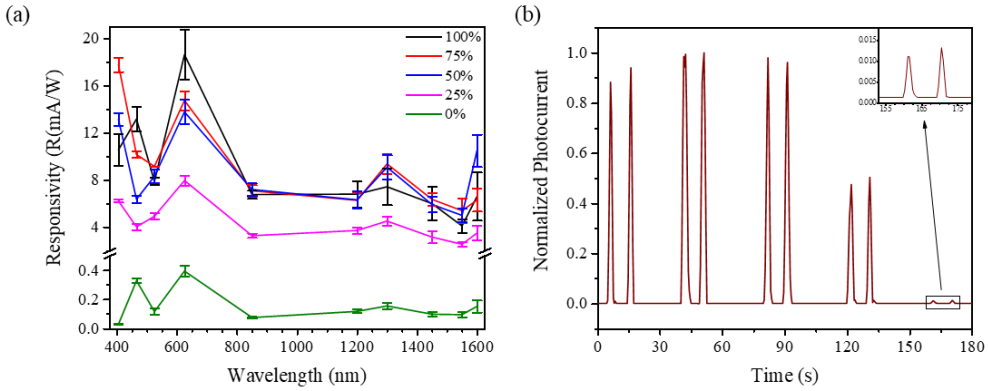

Figure 34. (a) Responsivity of the PEDOT:PSS percolated MWCNT based devices. (b) Spectral response of 0%, 25%, 50%, 75% and 100% PEDOT percolated CNT devices illuminated with 850 nm light source

3.3.4. Effect of Zinc Oxide Doping

In order to alter the responsivity spectrum of the sensors, PEDOT:PSS based sensors were doped with ZnO NPs. Figure 35 shows the doping effect of PEDOT:PSS based sensors on J-V curve and responsivity. When responsivities were examined, it was valid to say that ZnO was not alter the responsivity characteristics of the device.

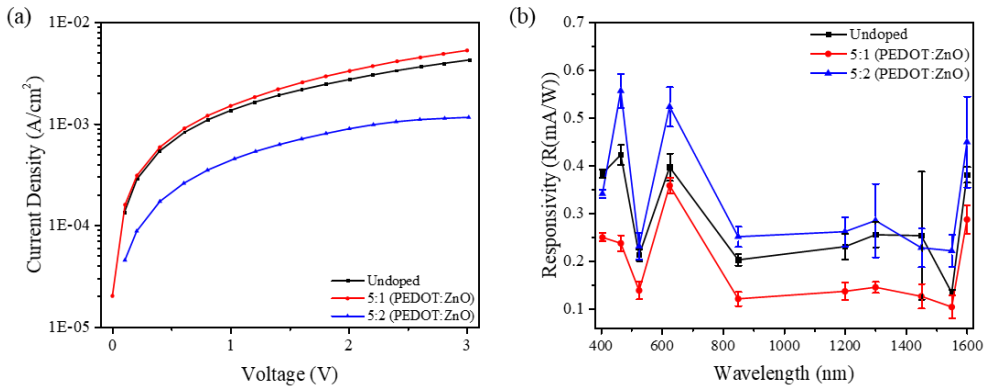

Figure 35. (a) Effect of the doping concentration of ZnO to J-V curve and (b) responsivity of represented devices

3.3.5. Acid Treatment of PEDOT:PSS

It is valid that PEDOT:PSS has core/shell structure both in aqueous solution and in the ready-prepared PEDOT:PSS film (Lang, Müller, Naujoks, & Dual, 2009). The shell is rich of hydrophilic PSS and the core is rich as hydrophobic PEDOT. By acidly treat the complex polymer structure, thickness of the less conductive shell is reduced to increase the charge transport across PEDOT chains. In other words, acid treatment reduces the Coulombic attraction between PEDOT and PSS. Thus, phase separation occurs between the hydrophobic PEDOT and hydrophilic PSS chains. The Coulombic attraction even disappears when the PSS chains become PSS—H chains by taking protons from other PSS chains. These PSS—H chains can segregate from PEDOT:PSS and be removed during the post-treatment rinse with water (Xia, Sun, & Ouyang, 2012).

PEDOT:PSS based sensors were treated with H_2SO_4 solution. Figure 36(a) shows the resistivity measurements of sensors before and after acid treatment. In order to perform acid treatment process, 10 µL of 0.2 M, 0.5 M and 1 M H_2SO_4 solution was drop-casted to PEDOT:PSS surface of each sensor. After the sensors were incubated at 80 ^oC for 10 minutes, they were pipetted with 40 µL of deionized water three times. Finally, they were incubated at 80 ^oC for 30 more minutes to evaporate residual deionized water. When the results were examined, resistivity drop was accomplished successfully; however, resistivity decrement should be observed at least one order of magnitude when compared the result studied by Xia and co-workers (Xia et al., 2012). For that purpose, same procedure was applied except incubating at 100 ^oC after drop casting H_2SO_4 solution and

pipetting processes. Figure 36(b) shows the resistivity measurements of PEDOT:PSS based sensors before and after acid treatment with 10 μL of 0.5 M and 1 M H_2SO_4 solution. Results indicated that increasing the incubation temperature to 100 ^oC could not enhance the resistivity to the intended level. Besides, concentration of H_2SO_4 solution should be higher in order to treat PEDOT:PSS.

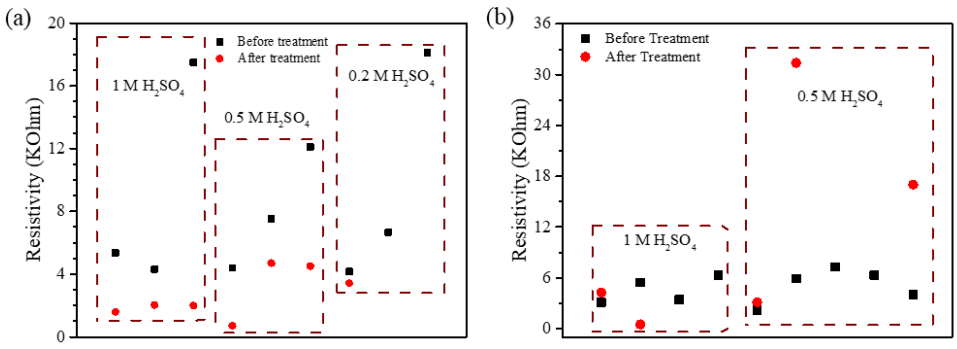

Figure 36. Resistivity comparison two failed acid treated PEDOT:PSS based sensors

After two failed acid treatment, Figure 37 shows the resistivity of the PEDOT:PSS based devices before and after treated by 1.0 M, 1.5 M and 2.0 M H_2SO_4 solution. The acid treatment was accomplished by incubating the sensors at 120 ^oC for 30 minutes. Furthermore, instead of pipetting with 40 μL of deionized water, they were submerged to deionized water. Results show that, after acid treatment, resistivities of the samples were measured as 10 times lower than those before treatment. Average resistivity of the sensors was calculated as 9.33 KOhm before treatment and 0.977 KOhm, 0.326 KOhm and 361 KOhm after 1.0 M, 1.5 M and 2.0 M H_2SO_4 treated, respectively. This dramatic change in resistivity indicates the successful removal of PSS from the conductive network.

3.4. Conjugated Polymer Based Free-Standing Composite Network for Volatilome Analyzer

Over the course of many years, there has been an increasing demand for low cost, portable, high sensing performance and reliable gas sensors that can detect low concentrations of analytes in real time. The detection of biological species with the aim of biosensors, microfluids and hand-held analyzers is a great concern in significant rela-

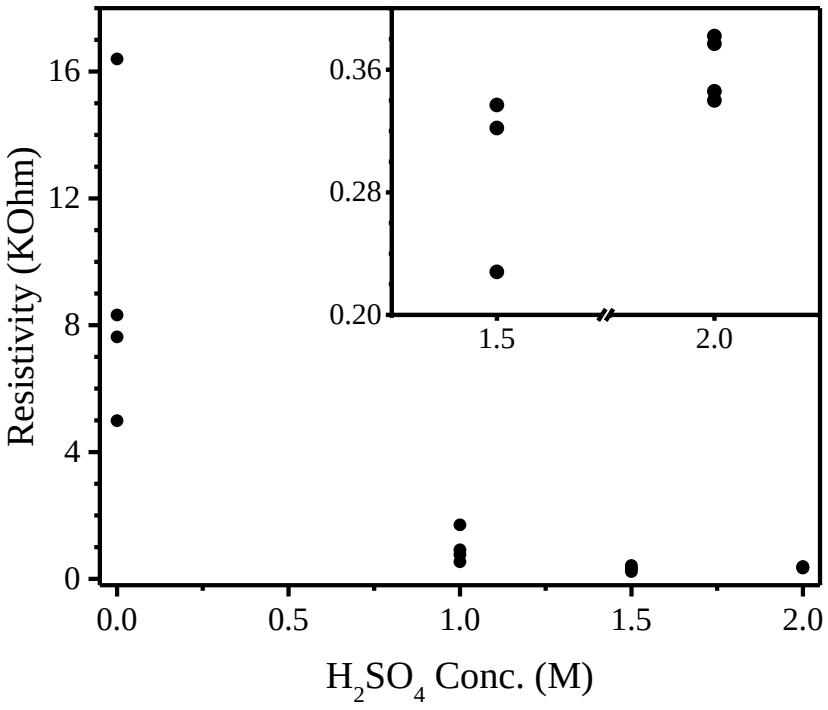

Figure 37. Resistivity comparison before and after acid treated PEDOT:PSS based sensors. 1.0 M, 1.5 M and 2.0 M H_2SO_4 solution was used for acid treatment

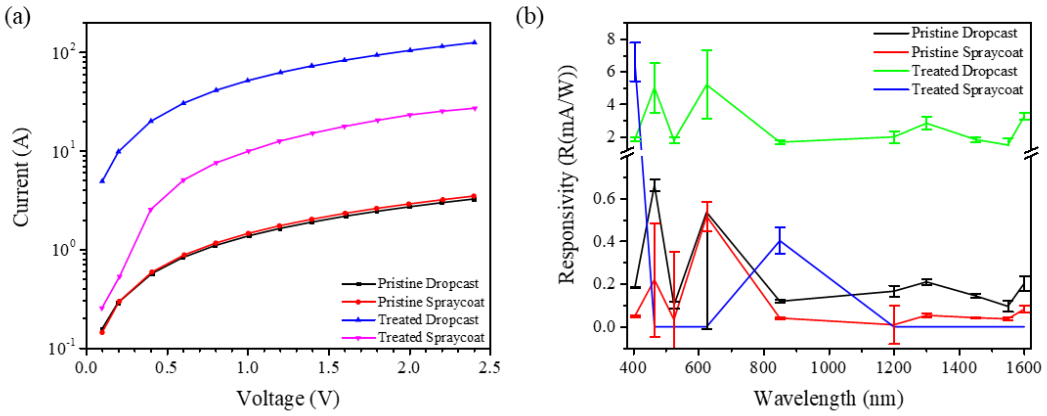

Figure 38. (a) J-V curves and (b) responsivity comparisons of acid treated and pristine devices prepared by drop-casting and spray-coating techniques

tion with medical diagnosis. Nano-engineered materials including one dimensional nano-structures (nanoribbons, nanowires and nanotubes) hold a great promise for sensor applications. Due to tunable electrical properties upon exposure to analytes, they have a good candidate for development and treatment breath analysis for diagnosis. In addition to this, studies inclined that nano-structure based sensor can separate VOCs which are correlates various diseases to human health.

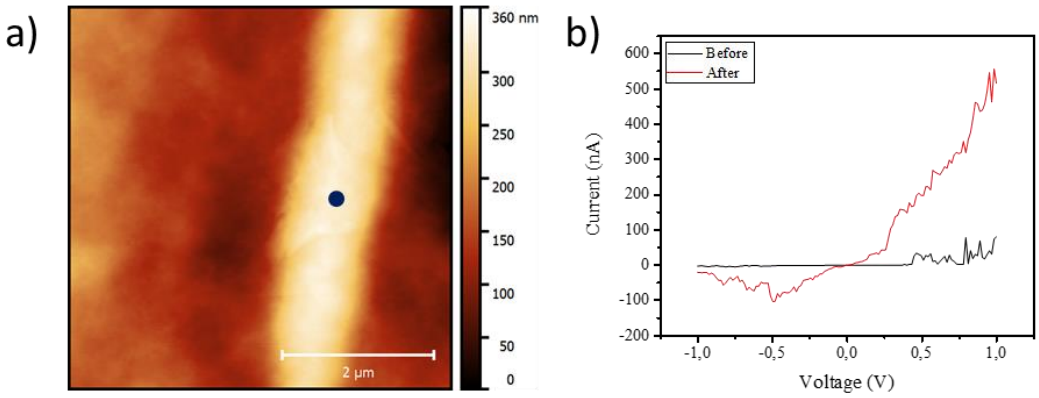

Figure 39. (b) Topography of AuNP doped PEDOT:PSS based conductive network which blue dot represents where (d) the I-V measurements were taken before (black line) and after (red line) ethanol exposure

Studying VOCs sensing characteristics both macroscopic and microscopic was an important concept to understand the sensing mechanism of the sensors. Figure 39(b) illustrates the I-V curves of the PEDOT:PSS based sensor before (black line) and after (red line) ethanol exposure that measured from the blue dot at Figure 39(a). Before ethanol gas exposure conductivity of the sensor on fiber was in the 50 nA range which was nearly no current flow. Once the sensor was exposed to ethanol gas, maximum observed current from the same point was at 500 nA level. There was an order of magnitude increment in the current when we compared before and after ethanol exposure.

Figure 40 summarize the VOCs responses of bare, AuNP and FeNP doped PEDOT:PSS sensors exposed to ethanol and acetone gases. When Figure 40(g-i) was examined, bare PEDOT:PSS based sensors were equally responsive to both acetone and ethanol as there were no selectivity. In the case of doping, AuNPs enhance responsivity

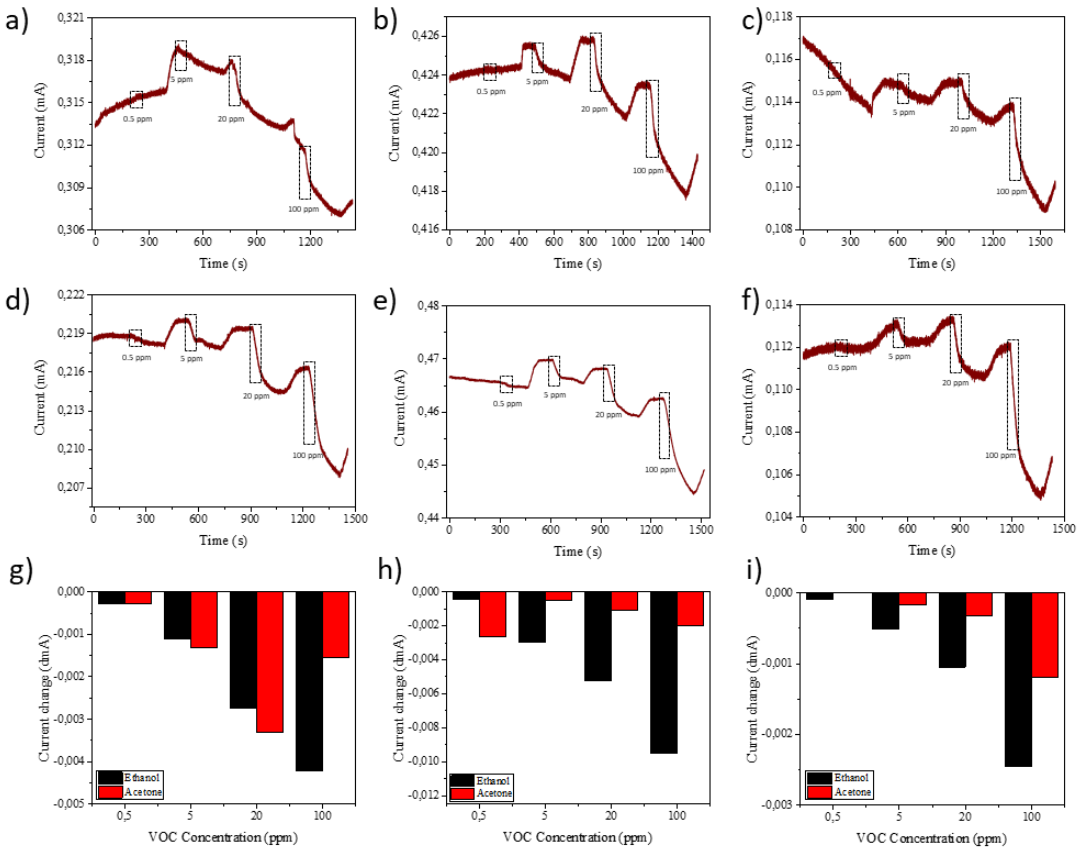

Figure 40. VOCs responses of (a, d) bare PEDOT:PSS, (b, e) AuNP doped PEDOT:PSS and (c, f) FeNP doped PEDOT:PSS gas sensors after exposing 0.5 ppm, 5 ppm, 20 ppm and 100 ppm (a-c) acetone and (d-f) ethanol. (g-i) Bar graphs shows the average current change of (g) Bare PEDOT:PSS, (h) AuNP doped PEDOT:PSS and (i) FeNP doped PEDOT:PSS sensors that calculated by 5 parallel gas sensors

to ethanol which was due to the increasement of interaction between VOC and conductive layer (Tasaltin & Basarir, 2014). In another case, FeNP decreases the response of acetone exposure as FeNP prevent acetone penetration through the conductive layer.

Figure 41 summarize the VOCs responses of bare, AuNP and FeNP doped MWCNT sensors exposed to ethanol and acetone gases. Comparison of MWCNT based sensors with PEDOT:PSS based sensors show that both conductive materials show similar VOC sensing characteristics. Apart from the similarities, MWCNT based sensors showed less noise level with and without VOC exposure that may due to higher base current.

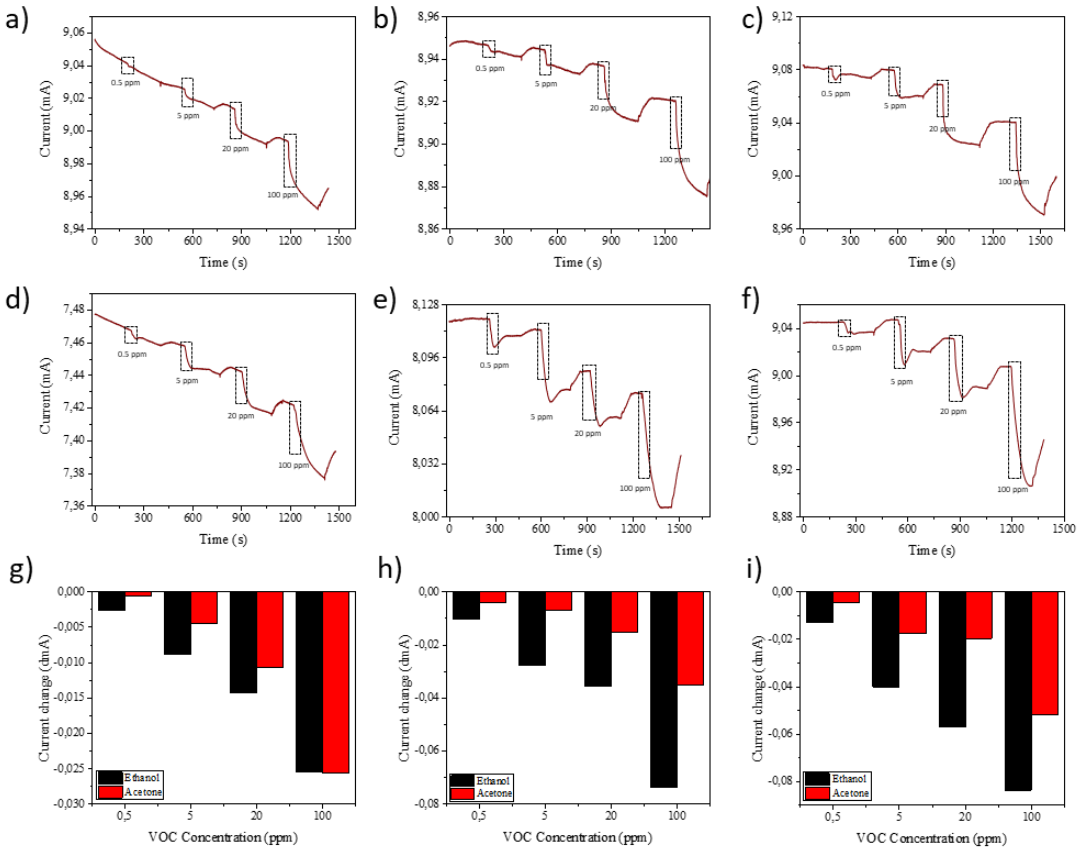

Figure 41. VOC responses of (a, d) bare MWCNT, (b, e) AuNP doped MWCNT and (c, f) FeNP doped MWCNT gas sensors after exposing 0.5 ppm, 5 ppm, 20 ppm and 100 ppm (a-c) acetone and (d-f) ethanol. (g-i) Bar graphs shows the average current change of (g) Bare MWCNT, (h) AuNP doped MWCNT and (i) FeNP doped MWCNT sensors that calculated by 5 similar gas sensors

CHAPTER 4

CONCLUSION

This thesis proposes an electrospun bendable substrate for copious sensor applications where some were explained and performed successfully. Conductive network was produced by drop-casting conductive material (MWCNT and PEDOT:PSS) through the free-standing PVDF surface. As a result, bendable network was fabricated which has resistivity from 100 Ω to 20 KΩ in order to use in many field from wearable electronics to medical diagnosis. First study describes noncontact sensing of human finger motion by conducting polymer electrospun nanofiber network free standing fabric type sensor platform. The moving object has been sensed through the electrostatic interactions between fibers and object and sensing range has been found to be 1-5 cm above the surface of fabric. The noncontact motion sensor platform has unique flexibility and light weight holding a potential for wearable sensor technology. In second study, low-consumption broadband photosensitive device was fabricated. PVDF nanofibers were acted as a substrate for acid treated MWCNT or PEDOT:PSS and PMMA was pedestal for the device. Conductive layer showed unexpected compatibility and form a highly conductive network with PVDF nanofibers that can be manipulated by irradiation. We further, investigate the effect of the concentration of conductive layer on photocurrent. In addition, studies showed that, obtained photo-resistors have broadband photoresponse from 400 nm to 1600 nm which makes it a promising competitor in telecommunication technologies. In the last work, to diagnose diabetes and cancer type diseases which can be diagnosed by volatilomes, POC type gas sensors were fabricated. In order to improve sensitivity and selectivity, conductive layer coated sensors were doped with AuNP and FeNP. Proposed methodology was concluded that there was a significant difference between undoped and doped sensors. This phenomenon was due to the altering effective surface to volume ratio via doping of conductive layer and effective electron donation to conductive layer lattice by gold and iron oxide nanoparticles. The interplay between gas molecules and nanoparticles were found to be major reason of selective response. This characteristic behavior of gas molecules is promising to build up conductive layer -

nanoparticle chemoresistor sensor arrays to quantitatively detect VOCs from human breath to design next generation volatilome analyzer.

REFERENCES

Adhikari, B., & Majumdar, S. (2004). Polymers in sensor applications. *Progress in Polymer Science, 29*(7), 699-766. doi:10.1016/j.progpolymsci.2004.03.002

Albanese, A., Tang, P. S., & Chan, W. C. W. (2012). The Effect of Nanoparticle Size, Shape, and Surface Chemistry on Biological Systems. *Annual Review of Biomedical Engineering, 14*(1), 1-16. doi:10.1146/annurev-bioeng-071811-150124

Alexeev, V. L., Sharma, A. C., Goponenko, A. V., Das, S., Lednev, I. K., Wilcox, C. S., Asher, S. A. (2003). High ionic strength glucose-sensing photonic crystal. *Analytical Chemistry, 75*(10), 2316-2323. doi:10.1021/ac030021m

Amal, H., Shi, D.-Y., Ionescu, R., Zhang, W., Hua, Q.-L., Pan, Y.-Y., Haick, H. (2015). Assessment of ovarian cancer conditions from exhaled breath. *International Journal of Cancer, 136*(6), E614-E622. doi:10.1002/ijc.29166

Bloor, D., & Movaghar, B. (1983). Conducting polymers. *IEE Proceedings I - Solid-State and Electron Devices, 130*(5), 225-232. doi:10.1049/ip-i-1.1983.0041

Carr, J. J. (1993). *Sensors and circuits : sensors, transducers, and supporting circuits for electronic instrumentation, measurement, and control*: PTR Prentice Hall.

Cichosz, S., Masek, A., & Zaborski, M. (2018). Polymer-based sensors: A review. *Polymer Testing, 67*, 342-348. doi:10.1016/j.polymertesting.2018.03.024

D'Amico, A., Bono, R., Pennazza, G., Santonico, M., Mantini, G., Bernabei, M., Di Natale, C. (2008). Identification of melanoma with a gas sensor array. *Skin Research and Technology, 14*(2), 226-236. doi:10.1111/j.1600-0846.2007.00284.x

Daneshkhah, A., Shrestha, S., Agarwal, M., & Varahramyan, K. (2015). Poly(vinylidene fluoride-hexafluoropropylene) composite sensors for volatile organic compounds detection in breath. *Sensors and Actuators B: Chemical, 221*, 635-643. doi:https://doi.org/10.1016/j.snb.2015.06.145

Delcea, M., Mohwald, H., & Skirtach, A. G. (2011). Stimuli-responsive LbL capsules and nanoshells for drug delivery. *Advanced Drug Delivery Reviews, 63*(9), 730-747. doi:10.1016/j.addr.2011.03.010

Doshi, J., & Reneker, D. H. (1995). Electrospinning process and applications of electrospun fibers. *Journal of Electrostatics, 35*(2), 151-160. doi:https://doi.org/10.1016/0304-3886(95)00041-8

Drummond, T. G., Hill, M. G., & Barton, J. K. (2003). Electrochemical DNA sensors. *Nature Biotechnology, 21*(10), 1192-1199. doi:10.1038/nbt873

Gong, X., Tong, M., Xia, Y., Cai, W., Moon, J. S., Cao, Y., Heeger, A. J. (2009). High-Detectivity Polymer Photodetectors with Spectral Response from 300 nm to 1450 nm. *Science, 325*(5948), 1665-1667. doi:10.1126/science.1176706

Hermanowicz, P., Sarna, M., Burda, K., & Gabryś, H. (2014). AtomicJ: An open source software for analysis of force curves. *Review of Scientific Instruments, 85*(6), 063703. doi:10.1063/1.4881683

Hu, J., & Liu, S. (2010). Responsive Polymers for Detection and Sensing Applications: Current Status and Future Developments. *Macromolecules, 43*(20), 8315-8330. doi:10.1021/ma1005815

Huang, Z. M., Zhang, Y. Z., Kotaki, M., & Ramakrishna, S. (2003). A review on polymer nanofibers by electrospinning and their applications in nanocomposites. *Composites Science and Technology, 63*(15), 2223-2253. doi:10.1016/s0266-3538(03)00178-7

Iijima, S. (1991). Helical microtubules of graphitic carbon. *Nature, 354*(6348), 56-58. doi:10.1038/354056a0

Janata, J., & Josowicz, M. (2003). Conducting polymers in electronic chemical sensors. *Nature Materials, 2*(1), 19-24. doi:10.1038/nmat768

Kan, E., Yang, J., & Li, Z. (2011). *Graphene Nanoribbons: Geometric, Electronic, and Magnetic Properties*: INTECH Open Access Publisher.

Lang, U., Müller, E., Naujoks, N., & Dual, J. (2009). Microscopical Investigations of PEDOT:PSS Thin Films. *Advanced Functional Materials, 19*(8), 1215-1220. doi:10.1002/adfm.200801258

Lange, U., Roznyatouskaya, N. V., & Mirsky, V. M. (2008). Conducting polymers in chemical sensors and arrays. *Analytica Chimica Acta, 614*(1), 1-26. doi:10.1016/j.aca.2008.02.068

Li, J., Lu, Y. J., Ye, Q., Cinke, M., Han, J., & Meyyappan, M. (2003). Carbon nanotube sensors for gas and organic vapor detection. *Nano Letters, 3*(7), 929-933. doi:10.1021/nl034220x

Lin, P., & Yan, F. (2012). Organic Thin-Film Transistors for Chemical and Biological Sensing. *Advanced Materials, 24*(1), 34-51. doi:10.1002/adma.201103334

Montuschi, P., Santonico, M., Mondino, C., Pennazza, G., Mantini, G., Martinelli, E., D'Amico, A. (2010). Diagnostic Performance of an Electronic Nose, Fractional Exhaled Nitric Oxide, and Lung Function Testing in Asthma. *CHEST, 137*(4), 790-796. doi:10.1378/chest.09-1836

Mutlu, M. U., Akin, O., & Yildiz, U. H. (2018). Polymer nanofiber-carbon nanotube network generating circuits. In C. E. Tabor, F. Kajzar, T. Kaino, & Y. Koike (Eds.), *Organic Photonic Materials and Devices Xx* (Vol. 10529).

Peng, G., Tisch, U., Adams, O., Hakim, M., Shehada, N., Broza, Y. Y., Haick, H. (2009). Diagnosing lung cancer in exhaled breath using gold nanoparticles. *Nature Nanotechnology, 4*, 669. doi:10.1038/nnano.2009.235

Peng, G., Tisch, U., & Haick, H. (2009). Detection of Nonpolar Molecules by Means of Carrier Scattering in Random Networks of Carbon Nanotubes: Toward

Diagnosis of Diseases via Breath Samples. *Nano Letters, 9*(4), 1362-1368. doi:10.1021/nl8030218

Peng, S., & Cho, K. (2003). Ab Initio Study of Doped Carbon Nanotube Sensors. *Nano Letters, 3*(4), 513-517. doi:10.1021/nl034064u

Rao, H., Liu, Y., Zhong, J., Zhang, Z., Zhao, X., Liu, X., Wang, Y. (2017). Gold Nanoparticle/Chitosan@N,S Co-doped Multiwalled Carbon Nanotubes Sensor: Fabrication, Characterization, and Electrochemical Detection of Catechol and Nitrite. *ACS Sustainable Chemistry & Engineering, 5*(11), 10926-10939. doi:10.1021/acssuschemeng.7b02840

Richter, A., Paschew, G., Klatt, S., Lienig, J., Arndt, K. F., & Adler, H. J. P. (2008). Review on hydrogel-based pH sensors and microsensors. *Sensors, 8*(1), 561-581. doi:10.3390/s8010561

Someya, T., Sekitani, T., Iba, S., Kato, Y., Kawaguchi, H., & Sakurai, T. (2004). A large-area, flexible pressure sensor matrix with organic field-effect transistors for artificial skin applications. *Proceedings of the National Academy of Sciences of the United States of America, 101*(27), 9966-9970. doi:10.1073/pnas.0401918101

Tasaltin, C., & Basarir, F. (2014). Preparation of flexible VOC sensor based on carbon nanotubes and gold nanoparticles. *Sensors and Actuators B-Chemical, 194*, 173-179. doi:10.1016/j.snb.2013.12.063

Wilson, J. S. (2005). Sensor Technology Handbook. In J. S. Wilson (Ed.), *Sensor Technology Handbook* (pp. 1-20). Burlington: Newnes.

Xia, Y., Sun, K., & Ouyang, J. (2012). Solution-processed metallic conducting polymer films as transparent electrode of optoelectronic devices. *Adv Mater, 24*(18), 2436-2440. doi:10.1002/adma.201104795

Yucel, M., Akin, O., Cayoren, M., Akduman, I., Palaniappan, A., Liedberg, B., Yildiz, U. H. (2018). Hand-Held Volatilome Analyzer Based on Elastically Deformable Nanofibers. *Analytical Chemistry, 90*(8), 5122-5129. doi:10.1021/acs.analchem.7b05187

Zilberman, Y., Tisch, U., Pisula, W., Feng, X., Müllen, K., & Haick, H. (2009). Spongelike Structures of Hexa-peri-hexabenzocoronene Derivatives Enhance the Sensitivity of Chemiresistive Carbon Nanotubes to Nonpolar Volatile Organic Compounds of Cancer. *Langmuir, 25*(9), 5411-5416. doi:10.1021/la8042928